Published in : International Journal of Pharmaceutics (2021), vol. 610, 121205
DOI: https://doi.org/10.1016/j.ijpharm.2021.121205
Status : Postprint (Author's version)

NANOPARTICLE-CONTAINING ELECTROSPUN NANOFIBROUS SCAFFOLDS FOR SUSTAINED RELEASE OF SDF-1α

Rodolfo Molina-Peña[a,1], Muhammad Haji Mansor[a,b,1], Mathie Najberg[a,c], Jean-Michel Thomassin[b], Baya Gueza[a], Carmen Alvarez-Lorenzo[c], Emmanuel Garcion[a], Christine Jérôme[b], Frank Boury[a]

[a] *Univ Angers, Université de Nantes, Inserm, CRCINA, SFR ICAT, F-49000 Angers, France*
[b] *Center for Education and Research on Macromolecules (CERM), CESAM-UR, University of Liège, B-4000 Liège, Belgium*
[c] *Departamento de Farmacología, Farmacia y Tecnologia Farmacéutica, I+D Farma (GI-1645), Facultad de Farmacia, and Health Research Institute of Santiago de Compostela (IDIS), Universidade de Santiago de Compostela, 15782 Santiago de Compostela, Spain*

KEYWORDS : Stromal cell-derived factor-1α (SDF-1α) ; Poly(lactic-co-glycolic acid) (PLGA) ; nanoparticles ; Sustained release ; Electrospinning ; Chitosan nanofibrous scaffold ; Glioblastoma cell trap

ABSTRACT :

Chemokines such as stromal cell-derived factor-1α (SDF-1α) regulate the migration of cancer cells that can spread from their primary tumor site by migrating up an SDF-1α concentration gradient, facilitating their local invasion and metastasis. Therefore, the implantation of SDF-1α-releasing scaffolds can be a useful strategy to trap cancer cells expressing the CXCR4 receptor. In this work, SDF-1α was encapsulated into poly(lactic-co-glycolic acid) (PLGA)-based nanoparticles and subsequently electrospun with chitosan to produce nanofibrous scaffolds of average fiber diameter of 261 ± 45 nm, intended for trapping glioblastoma (GBM) cells. The encapsulated SDF-1α maintained its biological activity after the electrospinning process as assessed by its capacity to induce the migration of cancer cells. The scaffolds could also provide sustained release of SDF-1α for at least 5 weeks. Using NIH3T3 mouse fibroblasts, human Thp-1 macrophages, and rat primary astrocytes we showed that the scaffolds possessed high cytocompatibility *in vitro*. Furthermore, a 7-day follow-up of Fischer rats bearing implanted scaffolds demonstrated the absence of adverse effects *in vivo*. In addition, the nanofibrous structure of the scaffolds provided excellent anchoring sites to support the adhesion of human GBM cells by extension of their pseudopodia. The scaffolds also demonstrated slow degradation kinetics, which may be useful in maximizing the time window for trapping GBM cells. As surgical resection does not permit a complete removal of GBM tumors, our results support the future implantation of these scaffolds into the walls of the resection cavity to evaluate their capacity to attract and trap the residual GBM cells in the brain.

Published in : International Journal of Pharmaceutics (2021), vol. 610, 121205
DOI: https://doi.org/10.1016/j.ijpharm.2021.121205
Status : Postprint (Author's version)

1. Introduction

Stromal cell-derived factor-1α (SDF-1α) is a 68-amino-acid chemokine (De La Luz Sierra et al., 2004) with a strong binding affinity to the C-X-C chemokine receptor type 4 (CXCR4) (Kofuku et al., 2009). One of its prominent physiological functions is to induce the migration of CXCR4-expressing stem and progenitor cells from the bone marrow towards a site of injury to initiate the process of tissue repair and recovery (Ratajczak et al., 2004). The directed migration is an effect of an elevated SDF-1α expression at the injury site (Deng et al., 2011; Kitaori et al., 2009; Knerlich-Lukoschus et al., 2010) and the simultaneous increase in SDF-1α degradation in the bone marrow (Jin et al., 2008; Marquez-Curtis et al., 2008) that creates a positive SDF-1α concentration gradient towards the site needing repair. In addition to its role in tissue regeneration, SDF-1α-induced chemotaxis also mediates the spreading of cancer cells that escaped their respective primary tumor sites. CXCR4-expressing cancer cells have been shown to penetrate the blood or lymphatic circulation and subsequently be chemoattracted to SDF-1 α-secreting organs such as the liver (Kim et al., 2006), bone marrow (Roccaro et al., 2014) and lymph nodes (Katsura et al., 2018) for future metastatic colonization. Even in non-metastasizing cancers, the chemotactic effect of SDF-1« can support tumor progression by facilitating the invasion of cancer cells into proximal healthy tissues (Zagzag et al., 2008). The significant influence of SDF-1α on the migration of cancer cells has motivated the design of implants capable of releasing this chemokine to create a local concentration gradient that may attract CXCR4-expressing cancer cells relevant to many types of cancers including glioblastoma (GBM) (Carmo et al., 2010), melanoma (O'Boyle et al., 2013) and breast cancer (Sobolik et al., 2014).

Like other peptides and proteins, SDF-1α is water-soluble and thus can move rapidly through a physiological fluid compartment (Pardridge, 2011). Therefore, to establish and maintain a local concentration gradient of SDF-1α, sustained delivery of this chemokine from a fixed source is necessary. In this regard, encapsulation into nanocarriers composed of biodegradable polymers is a reasonable strategy to achieve gradual release of active molecules at the intended site of delivery (Almouazen et al., 2012; Hamoudeh et al., 2007; Nicolas et al., 2018). We have previously encapsulated SDF-1α into poly-(lactic-co-glycolic acid) (PLGA) nanoparticles (NPs) (Haji Mansor et al., 2018). However, we showed that the duration of SDF-1α release resulting from this approach was relatively brief. The release profile showed a steep initial release curve that leveled out shortly afterwards and that is characteristic of this kind of NPs with a two phase process where the first phase of "burst release" from locations near the NP's surface is followed by a second phase of prolonged release from the core compartment (Martinez Rivas et al., 2017). In addition, NPs tend to spread away from the initial site of application, making it difficult to establish a concentration gradient of the released drug molecules. Considering these shortcomings, we postulate that the SDF-1α-loaded NPs should be embedded within a suitable scaffold to slow down the SDF-1α release process and to prevent them from moving away from the initial site of administration.

Currently, there are multiple types of scaffolds within which drug-loaded carriers can be confined. These structures can provide an additional barrier to the drug diffusion process and may subsequently contribute to a longer duration of drug release from the primary carrier into the local

Published in : International Journal of Pharmaceutics (2021), vol. 610, 121205
DOI: https://doi.org/10.1016/j.ijpharm.2021.121205
Status : Postprint (Author's version)

environment. These include physically and chemically cross-linked hydrogels (Lee et al., 2018; Ono et al., 2017; Zhang et al., 2016), scaffolds prepared by the freeze-drying process (Gentile et al., 2015; Najberg et al., 2020; Pulavendran and Thiyagarajan, 2011) and those derived from a direct compression of the drug-loaded carriers (Du et al., 2017). However, these confining matrices usually lack the nano-fibrous structures typically found in native human extracellular matrices (ECM). In relation to our objective, it is important to develop scaffolds with structures mirroring those of the ECM in order to promote the adhesion and retention of cancer cells. In this regard, nanofibrous scaffolds can be prepared using electrospinning (Huang et al., 2003; Pham et al., 2006). Many natural and synthetic materials can be used to produce electrospun ECM-mimetic nanofibrous scaffolds. Among these, chitosan has been an outstanding material for making electrospun scaffolds to be used in a variety of biomedical applications due to its excellent biocompatibility (Frohbergh et al., 2012; Ma et al., 2011; Xie et al., 2013). Nevertheless, the electrospinning of chitosan and many other materials involves challenging conditions, including the use of high voltage to draw fibers from the material solution, which may compromise the structural integrity of protein molecules pre-incorporated into the solubilized material (Bekard and Dunstan, 2013; Toschi et al., 2009; Wang et al., 2014; Zhao and Yang, 2010, 2009). Therefore, we hypothesize that by pre-encapsulating SDF-1α molecules into PLGA-based NPs, their denaturation during processing may be minimized.

In the present study, SDF-1α was encapsulated into NPs composed of PLGA and a polyethylene glycol (PEG)-PLGA co-polymer. The SDF-1α-loaded NPs were then dispersed in a chitosan solution in the presence of the fiber-forming additive polyethylene oxide (PEO) and subsequently electrospun to produce NP-containing nanofibrous scaffolds. After electrospinning, the charged chitosan amino groups within the nanofibers were deprotonated to improve the scaffold stability in physiological media. Following this, the *in vitro* release patterns of the model protein lysozyme as well as of SDF-1α from the scaffolds were studied. The bioactivity of the released SDF-1α was subsequently evaluated by assessing its capacity to induce the migration of CXCR4-expressing human GBM cells (U87-MG). Finally, after studying their degradation profiles, the scaffolds' ability to retain U87-MG cells as well as their cytocompatibility was assessed *in vitro* and *in vivo* to evaluate the appropriateness of their use in future *in vivo* studies.

2. Materials and methods

2.1. MATERIALS

Ester-capped PLGA (Mn = 5.5 kDa) and PEG-PLGA copolymer (Mn_{PEG} = 5 kDa, Mn_{PLGA} = 25.7 kDa) were synthesized using a ringopening polymerization method as described elsewhere (Haji Mansor et al., 2018). Glycofurol (Tetraglycol BioXtra®), isosorbide dimethyl ether, poloxamer 188 (Lutrol® F68), sodium chloride, lysozyme from hen egg white, glycine, 10 M sodium hydroxide, dimethyl sulfoxide, Tris base (Trizma®), 37% hydrochloric acid, *Micrococcus lysodeikticus*, low gelling point agarose and PEO (average Mv ~ 2 MDa) were obtained from Sigma-Aldrich (Saint Quentin Fallavier, France). Human SDF-1α (research grade) was purchased from Miltenyi Biotech (Paris, France), chitosan with

Published in : International Journal of Pharmaceutics (2021), vol. 610, 121205
DOI: https://doi.org/10.1016/j.ijpharm.2021.121205
Status : Postprint (Author's version)

a degree of deacetylation of ~ 80% and molecular weight ~ 10 - 50 kDa (Chitoceuticals®) from Heppe Medical Chitosan GmbH (Halle, Germany), 1X Dulbecco's phosphate-buffered saline (Biowhittaker®) from Lonza (Verviers, Belgium), bovine serum albumin fraction V from Roche Diagnostics GmbH (Mannheim, Germany) and high glucose Dulbecco's Modified Eagle's Medium (Gibco®) from Thermo Fisher Scientific (Villebon sur Yvette, France). Deionized water supply was obtained from a Milli-Q® Advantage A10 system (Millipore, Paris, France).

2.2. PREPARATION AND CHARACTERIZATION OF PROTEIN-LOADED NANOPARTICLES

2.2.1. PREPARATION OF PROTEIN-LOADED NANOPARTICLES

Protein-loaded NPs were prepared as described previously (Haji Mansor et al., 2018). Briefly, the lyophilized model protein lysozyme and SDF-1α as provided by their respective manufacturers were separately dissolved in 0.15 M sodium chloride (NaCl) solution containing 20% w/v poloxamer 188 at a concentration of 10 and 1.33 mg/mL, respectively. After that, 975 µL of glycofurol was added to 25 µL of the lysozyme solution, and 185 µL of glycofurol to 15 µL of the SDF-1α solution. A smaller volumetric ratio of glycofurol to SDF-1α solution was used for convenience and worked well as SDF-1α is less soluble than lysozyme in aqueous solutions. The mixtures were subsequently incubated in ice for 30 min to induce the formation of protein precipitates. Then, 100 µL of the protein precipitate dispersion containing either 25 µg lysozyme or 10 µg SDF-1α was mixed with 100 µL of a 12% w/v PEG-PLGA solution and 200 µL of a 12% w/v PLGA solution in isosorbide dimethyl ether (total volume after mixing was 400 µL). Using Equation (1), the theoretical drug loadings (DL) for lysozyme and SDF-1α were calculated to be 0.07% and 0.03% respectively. For the synthesis of unloaded NPs, the 100 µL protein precipitate dispersion was replaced with an equal volume of glycofurol alone. Then, 2.1 mL of 0.05 M glycine-sodium hydroxide buffer solution was added gradually under magnetic stirring to initiate the formation of NPs that encapsulated the protein load. As the solubilities of lysozyme and SDF-1α were reduced as the pH of their respective solutions reached their protein isoelectric points (pI) (pI lysozyme = 11.35; pI SDF-1α = 10.5), a greater encap-sulation efficiency was achieved. Therefore, the pH of the buffer solution was set to 11.35 and 10.40 for the encapsulation of lysozyme and SDF-1α, respectively. The formed nanoparticle (NP) dispersion was subsequently diluted with excess deionized water and agitated under slow magnetic stirring for 1 h to wash out solvents and unencapsulated proteins. The suspended NPs were then centrifuged for 30 min at 10,000 × g, and the supernatant was discarded and replaced with an equal volume of deionized water. The centrifugation was repeated once and after subsequent removal of the supernatant, the purified NP dispersion was stored at a concentration of approximately 40 mg/mL in 0.5 mL volume in deionized water at 4 °C until use.

$$DL(\%) = \frac{Initial\ mass\ of\ protein\ used\ as\ a\ starting\ material}{Total\ mass\ of\ PLGA\ and\ PEG{-}PLGA} \times 100 \quad (1)$$

Published in : International Journal of Pharmaceutics (2021), vol. 610, 121205
DOI: https://doi.org/10.1016/j.ijpharm.2021.121205
Status : Postprint (Author's version)

2.2.2. CHARACTERIZATION OF PROTEIN-LOADED NANOPARTICLES

The morphology of the NPs was visualized using scanning electron microscopy (SEM) (JSM6310F, JEOL, Paris, France). The purified NP dispersion was initially diluted 200-fold with deionized water to a concentration of approximately 200 µg/mL. Then, 2 µL of the dispersion was added onto a glass slide and left overnight to dry at room temperature. Prior to observation, a gold coating of 5 nm thickness was deposited onto the NP sample.

The size distribution of the NPs was determined using a dynamic light scattering (DLS) method whereas zeta-potentials were derived from the electrophoretic mobility values using the Smoluchowski's approximation in a Nanosizer® ZS (Malvern, Worcestershire, UK). Initially, the purified NP dispersion was diluted with either deionized water or 0.01 M NaCl solution (pH was adjusted to 7 prior to measurement) for size and zeta-potential measurements, respectively, to obtain optimal NP concentrations for analyses such that the attenuator values were in the range of 5-7. Each sample was measured three times, with one measurement representing the average value of at least 10 runs. All measurements were conducted at 25 °C under the automatic mode. In addition to the average particle size, the DLS protocol of Nanosizer® ZS generated a polydispersity index (PDI) ranging from 0 to 1 that estimates the width of the size distribution.

For the assessment of protein encapsulation efficiencies, the protein- loaded NPs were initially lyophilized for 16 h alongside the unloaded NPs that served as a control. Then, the NPs were dissolved in 1 mL of dimethyl sulfoxide. After 1 h, 3 mL of 0.01 M hydrochloric acid (HCl) was added to extract the protein load from the polymeric components of the NPs. The samples were then diluted appropriately prior to assessment using the protein quantification assays described in Section 2.6. The encapsulation efficiency (EE) was calculated using Eq. (2).

$$EE(\%) = \frac{Mass\ of\ protein\ recovered\ from\ dissolved\ nanoparticles}{Initial\ mass\ of\ protein\ used\ as\ a\ starting\ material} \times 100 \quad (2)$$

2.3. PREPARATION AND CHARACTERIZATION OF NANOPARTICLE-CONTAINING NANOFIBROUS SCAFFOLDS

2.3.1. PREPARATION OF NANOPARTICLE-CONTAINING NANOFIBROUS SCAFFOLDS

To prepare nanofibrous scaffolds containing protein-loaded NPs, 11 mg of PEO was initially added to 0.5 mL of NP dispersion in deionized water. The NP concentration was varied between 10 and 40 mg/mL to determine the maximum mass of NPs that can be loaded into the nanofibrous scaffolds. After that, the NPs/PEO mixture was added to 1.7 mL of 6.5% w/v chitosan solution in 1 M acetic acid. Based on this, the theoretical NP load in the nanofibrous scaffold to be synthesized ranged from 4.0 to 14.2% w/w (5-20 mg NPs per 110 mg chitosan and 11 mg PEO). The materials were then mixed at room temperature using a laboratory magnetic stirrer set to 100 rpm for 2 h. For the preparation of nanofibrous scaffolds carrying unencapsulated protein molecules, the PEO was dissolved in 0.5 mL deionized water containing either 25 µg lysozyme or 10 µg SDF-1α to match the protein load in the NPs prior to mixing with the 6.5% w/v chitosan solution. The homogenized materials were subsequently transferred into a 10 mL HSW SOFT-JECT® disposable plastic syringe (Henke-Sass,

Published in : International Journal of Pharmaceutics (2021), vol. 610, 121205
DOI: https://doi.org/10.1016/j.ijpharm.2021.121205
Status : Postprint (Author's version)

Wolf GmbH, Tuttlingen, Germany) with a luer slip tip that was fixed with a 21 G × 1½ in blunt-ended needle. The syringe was then left to stand for another 2 h for degassing.

For the electrospinning step, the syringe containing the protein-loaded NPs, PEO and chitosan was carefully mounted onto a syringe driver (KD Scientific, Holliston, MA, USA) with the tip of the needle positioned 17 cm away from the collector plate. The syringe driver was used to control the flow rate of the materials at 0.78 mL/h. To produce nanofibers, a Spellman SL10® high voltage generator (Spellman High Voltage Electronics Corp., Hauppauge, NY, USA) was used to apply a potential difference of 30 kV between the needle and the collector plate for 165 min. The nanofibers were deposited onto a piece of aluminum foil covering the collector plate to facilitate the subsequent retrieval of the electrospun scaffold.

2.3.2. CHARACTERIZATION OF NANOPARTICLE-CONTAINING NANOFIBROUS SCAFFOLDS

The thickness of the nanofibrous scaffolds were measured using a Kaefer Dial Gauge (Kaefer Messuhrenfabrik GmbH, Villingen-Schwenningen, Germany).

The composition of the nanofibrous scaffolds was determined using attenuated total reflectance-Fourier transform infrared (ATR-FTIR) spectroscopy. ATR-FTIR spectra were recorded using a Nicolet iS5® spectrometer (Thermo Fisher Scientific) with a spectral resolution of 4 cm^{-1}.

The morphology of the nanofibrous scaffolds was observed using scanning electron microscopy (SEM) (JSM 840A, JEOL) and transmission electron microscopy (TEM) (JEM 1400, JEOL). For SEM, the nanofibrous scaffolds were coated with a 5 nm platinum layer prior to observation. Fiber diameter measurements were then performed using the ImageJ software (NIH, USA) on 30 randomly selected fibers in a SEM image. Three SEM images were analyzed for each sample. For TEM, nanofibers were collected on a copper grid (Gilder Grids, Grantham, UK) placed in front of the collector plate for about 3 s during the electrospinning process and observed without any coating.

To investigate whether the electrospinning process contributes to any protein denaturation, 2 mL of 1 M acetic acid solution was added to the nanofibrous scaffolds to dissolve the nanofibers and subsequently release the protein-loaded NPs. After 1 h, 4 mL of a 1 M NaOH solution was added gradually to increase the basicity of the mixture (to pH > 13) to induce the precipitation of the chitosan molecules as well as the dissolution of the NPs. After another 1-h incubation, the mixture was centrifuged at 9500 × g for 30 min to spin down the chitosan precipitates. 2 mL of the supernatant was kept for use in the protein quantification assays described in Section 2.6.

2.4. STABILIZATION OF THE NANOFIBROUS SCAFFOLDS

To reduce the solubility of the nanofibrous scaffolds in physiological media, the charged amino groups of chitosan in the nanofibers were deprotonated (He et al., 2011; Tchemtchoua et al., 2011). To achieve this, the nanofibrous scaffolds were treated sequentially with absolute ethanol for 5 min and then 0.1 M NaOH for 30 s, followed by three times washing with 0.1X phosphate-buffered saline (PBS) (pH 7.4). The scaffolds were then dried under reduced pressure for 16 h.

Published in : International Journal of Pharmaceutics (2021), vol. 610, 121205
DOI: https://doi.org/10.1016/j.ijpharm.2021.121205
Status : Postprint (Author's version)

2.5. IN VITRO PROTEIN RELEASE STUDY

The *in vitro* protein release study was conducted on the protein-loaded NPs, nanofibrous scaffolds loaded with unencapsulated protein molecules and protein-loaded NPs incorporated into nanofibrous scaffolds. Protein-free NPs and nanofibrous scaffolds were used as controls. All nanofibrous scaffolds were stabilized prior to use as described in section 2.4. NPs and whole scaffolds were incubated separately at 37 °C in 2 mL of 0.05 M Tris-HCl buffer solution (pH 7.4) supplemented with 0.15 M NaCl and 1 mg/mL bovine serum albumin (BSA) as a protein stabilizer. At each pre-defined time point, 1.5 mL of the buffer solution was collected and replaced with fresh buffer. For the NP samples, the dispersion was centrifuged at 9,500 × g for 30 min to spin down the NPs and 1.5 mL of the supernatant was subsequently collected and replaced with fresh buffer. The quantification of protein molecules in the collected samples was conducted as described in Section 2.6.

2.6. PROTEIN QUANTIFICATION

2.6.1. QUANTIFICATION OF LYSOZYME

Lysozyme was quantified using the turbidity reduction assay as described by Hassani and colleagues (Hassani et al., 2013). Briefly, 100 µL of lysozyme-containing sample was added to 2.9 mL of 0.015% w/v *Micrococcus lysodeikticus* suspension in 0.05 M Tris-HCl buffer solution (pH 7.4). The assay mixture was then incubated at 37 °C to allow the lysozyme molecules to lyse the *M. lysodeikticus* cell walls. After 4 h, the absorbance at 450 nm was measured (Multiskan Ascent, Labsystems, Les Ulis, France). To construct a standard curve, lysozyme solutions of concentration ranging from 100 to 1000 ng/mL were also assayed. Each sample was diluted with 0.05 M Tris-HCl buffer solution (pH 7.4) by several dilution factors to obtain absorbance readings that were within the standard curve range.

2.6.2. QUANTIFICATION OF SDF-1α

SDF-1α was quantified using an enzyme-linked immunosorbent assay (ELISA) as per supplier's instructions (R&D Systems, Lille, France). Briefly, a Nunc Maxisorp® 96-well microplate (Thermo Fisher Scientific) was incubated overnight with SDF-1α capture antibody solution to coat the wells. The plate was then washed with 0.05% w/v Tween® 20 in 1X PBS (pH 7.4). To prevent any non-specific protein binding during the sample incubation stage, the plate was subsequently incubated with 10 mg/mL BSA solution in 1X PBS (pH 7.4) for 1 h. After washing, SDF-1α-containing samples and the provided SDF-1α standard pre-diluted with 10 mg/mL BSA solution in 1X PBS (pH 7.4) were added to the wells for a 2-h incubation. Following another wash, the wells were incubated with detection antibody solution for 2 h. The plate was washed again prior to a 20-min incubation with streptavidin-horseradish peroxidase solution. The final washing step was carried out and the plate was then incubated with the substrate solution for another 20 min. The enzymatic reaction was subsequently terminated by adding 1 M sulfuric acid solution and the absorbance at 450 nm was immediately measured (Multiskan Ascent, Labsystems, Les Ulis, France). All incubations were done at room temperature.

Published in : International Journal of Pharmaceutics (2021), vol. 610, 121205
DOI: https://doi.org/10.1016/j.ijpharm.2021.121205
Status : Postprint (Author's version)

2.7. ASSESSMENT OF SDF-1α BIOACTIVITY

SDF-1α bioactivity was assessed using an agarose drop migration assay (Milner et al., 1996). Initially, constitutively CXCR4-expressing U87-MG cells, as produced by Séhédic and colleagues (Séhédic et al., 2017), were seeded into a 24-well flat-bottomed culture plate (Nunc, Strasbourg, France) at a density of 1×10^5 cells per well and incubated with Dulbecco's Modified Eagle's Medium (DMEM) supplemented with 10% fetal bovine serum (FBS) and 1% penicillin/streptomycin. To enhance cell adhesion, each well was previously treated with 500 µL of 10 µg/mL poly-D-lysine hydrobromide (Sigma-Aldrich) solution for 15 min and subsequently washed with 1X PBS three times. After 72 h of incubation, the medium was replaced with deionized water to lyse the cells. The wells were washed with 1X PBS after 20 min and the thin cell-derived matrices coating the well surfaces were left to air-dry under laminar flow. Next, 2 µL of 1% w/v solution of low gelling point agarose containing 1×10^5 CXCR4-expressing U87-MG cells was deposited onto the center of each well and the plate was kept at 4 °C for 15 min for the gelation step. Then, the cell-loaded agarose drop was covered with 400 µL of DMEM (FBS-free, 1% penicillin/streptomycin) with or without 40 ng/mL of native SDF-1α as controls; or with DMEM containing SDF-1α extractables from scaffolds after electrospinning or leached SDF-1α from the releasing studies. Three drops were assayed for each medium condition in each experiment. After 72 h, the plan view of each well was captured using an optical microscope and a built-in camera (AxioCam® ICm 1, Zeiss, Jena, Germany). The cell migration distance was estimated by measuring the distance between the edge of the drop and the cell front on four distinct sides of the drop using the ImageJ software. The measurements were subsequently averaged to obtain a representative migration distance in each well. All incubations were done at 37 °C and 5% CO_2.

2.8. IN VITRO SCAFFOLD DEGRADATION STUDY

Stabilized nanofibrous scaffolds were cut into quarters of approximately 25 mg in mass. The scaffold pieces were then incubated separately in 2 mL of 0.05 M Tris-HCl buffer solution (pH 7.4) supplemented with 0.15 M NaCl, 20 µg/mL lysozyme and 1 mg/mL BSA at 37 °C. At each pre-defined time point, three scaffold pieces were removed from their respective buffer solution using sterile tweezers, the excess liquid was blotted up using KIMTEC wipers, and the scaffolds were then dried in a desiccator under reduced pressure for 16 h. The dried scaffold pieces were then weighed, and the % of scaffold mass degraded throughout the incubation period was calculated using Eq. (3).

$$\%\ of\ scaffold\ mass\ degraded = \frac{mass\ before\ incubation - mass\ after\ incubation}{mass\ before\ incubation} \times 100\% \quad (3)$$

2.9. IN VITRO CYTOCOMPATIBILITY AND CELL ADHESION ASSAYS

To exclude any potential proliferative effect of the protein load that may reduce the reliability of the study results, only the nanofibrous scaffold loaded with blank NPs and the unloaded nanofibrous scaffold were evaluated in these assays. Two *in vitro* methods were used to evaluate the scaffold cytocompatibility: (a) a 24-h incubation of cells with scaffold leachables, and (b) a more realistic scenario in which cells were incubated with scaffolds for 24 and 72 h. All incubations were done at

Published in : International Journal of Pharmaceutics (2021), vol. 610, 121205
DOI: https://doi.org/10.1016/j.ijpharm.2021.121205
Status : Postprint (Author's version)

37 °C and 5% CO2 and the medium used was always supplemented with 10% FBS and 1% penicillin/streptomycin.

2.9.1. IN VITRO CYTOCOMPATIBILITY ASSAY

2.9.1.1. Indirect method

The *in vitro* cytocompatibility of the nano-fibrous scaffolds by the indirect test was assessed using the "scaffold extract" method adapted from Wang and colleagues (Wang et al., 2013). The nanofibrous scaffolds were cut into circular pieces of 10 mm in diameter and approximately 0.6 mg in mass to promote ease of handling. Five scaffold pieces were placed together in a well of a 24-well flat-bottomed culture plate (Nunc) containing 400 µL of DMEM and incubated for 24 h to produce the scaffold extract. Simultaneously, NIH3T3 mouse fibroblasts cells (CRL-1658™, ATCC, Rockville, Maryland, USA) were seeded in a 96-well flat-bottomed culture plate (Nunc) at a density of 5500 cells/well in 100 µL of DMEM and incubated for 24 h. Then, the medium on the cells was replaced with 100 µL of the scaffold extract and the cells were incubated for another 24 h. As a positive control, 100 µL of fresh medium was used in place of the scaffold extract. 10 µL of WST-1 reagent (Sigma-Aldrich) were subsequently added into each well. After 2 h of incubation, the number of viable cells was estimated from the absorbance of the cleaved product of the tétrazolium salts in the WST-1 reagent, called formazan, which was measured at 450 nm using a ClarioStar® microplate reader (BMG Labtech GmbH, Ortenberg, Germany). To estimate the background absorbance, the WST-1 reagent was also added to wells containing either the scaffold extract or fresh medium alone without any cells. All background-corrected absorbance values were normalized to those of the positive control.

2.9.1.2. Direct contact method

Contact-induced cytotoxicity of the nanofibrous scaffolds was assessed using NIH3T3 mouse fibroblasts, human Thp-1 macrophages, and rat primary astrocytes. Assays were conducted in 24-well cell culture plates (well diameter = 15.6 mm). All incubations were done at 37 °C and 5% CO2 and DMEM supplemented with 10% FBS and 1% penicillin/streptomycin was used throughout the assay unless stated otherwise.

Cells were prepared accordingly prior to the 24 or 72-h period of incubation with the scaffolds. NIH3T3 cells were seeded at a density of 40×10^3 and 10×10^3 cells/well for the 24 and 72-h assays respectively and incubated in 500 µL medium 24 h before use. To obtain Thp-1 macrophages, Thp-1 monocytes (TIB-202™, ATCC) were seeded at a density of 200×10^3 cells and 50×10^3 cells/well for the 24 and 72-h assays, respectively. The Thp-1 monocytes were incubated in 500 µL complete Roswell Park Memorial Institute (RPMI) 1640 medium (Sigma-Aldrich) supplemented with 80 nM phorbol 12-myristate 13-acetate (PMA) (Sigma-Aldrich) for 24 h to induce their differentiation into macrophages. Following this, the PMA-containing medium was replaced with fresh complete RPMI medium (without PMA) and the cells were incubated for another 24 h before use. Purified cultures of newborn rat primary astrocytes were prepared from extracts of cerebral cortex using the mechanical dissociation method as originally described (McCarthy and de Vellis, 1980). Brain extract was homogenized, lyophilized and reconstituted in cell culture medium before being added to the 24-

Published in : International Journal of Pharmaceutics (2021), vol. 610, 121205
DOI: https://doi.org/10.1016/j.ijpharm.2021.121205
Status : Postprint (Author's version)

well plate. The medium was refreshed twice weekly for two weeks to obtain highly pure cultures of primary astrocytes.

Prior to incubation with the cells, the nanofibrous scaffolds were cut into circular pieces of 10 or 14 mm in diameter, which correlated to a 2-fold difference in surface areas (79 vs. 154 mm^2, respectively). The scaffold pieces were washed with 1X PBS three times and incubated in the cell culture medium for 15 min before being deposited onto the cell monolayer prepared in the 24-well plate. Wells without scaffolds acted as control. After 24 or 72 h of incubation, the medium in each well was replaced with 500 µL fresh medium containing 44 µM resazurin. To estimate the background fluorescence, the resazurin-containing medium was also added into three empty wells of the assay plate (without any cells). The plate was incubated for another 2 h.

Cell viability was estimated from the fluorescence intensity of the reduced product of resazurin, called resorufin, which was measured using a ClarioStar microplate fluorometer (BMG Labtech GmbH, Ortenberg, Germany) at 545 nm excitation and 600 nm emission. All background-corrected fluorescence intensity values were normalized to those obtained with the control wells.

2.9.2. IN VITRO CELL ADHESION ASSAY

The cell adhesion capacity of the nanofibrous scaffolds was studied using U87-MG cells (HTB-14™, ATCC). Initially, 25 µL of DMEM containing 1 x 10^4 cells was deposited on the top of a scaffold piece placed in a well of a 48-well flat-bottomed culture plate (Nunc). As a positive control, the same number of cells was added to a well without any scaffold. After 1 h of incubation, another 275 µL of medium was added into the wells and the plate was incubated for another 3 h to allow the cells to adhere to the scaffold or well surfaces. Then, the wells were washed with 1X PBS three times to remove any loosely attached cells. After another 24 h of incubation in 300 µL of fresh medium, the cell viability on the scaffold was evaluated using WST-1 reagent as described in Section 2.9.1.1. To ensure that the cells that reacted with the WST-1 reagent were those that were attached to the scaffolds and not of any colonies that formed on the well surface underneath, the scaffolds were transferred into new wells containing 300 µL of fresh medium before adding 30 µL of WST-1 reagent. To determine the background absorbance, the reagent was also added to cell-free wells containing DMEM with or without a scaffold piece. For the absorbance measurement, 100 µL of medium was transferred from each well to a 96-well plate 2 h after the addition of WST-1 reagent.

For the SEM analysis, the scaffolds were washed three times with PBS and equilibrated in DMEM. Then a 25 µL drop containing 2 × 10^4 cells was deposited on top of the scaffolds. After 1 h incubation at 37 °C, 275 µL of DMEM was added and the scaffolds incubated during 72 h. The scaffolds were then fixed in a 0.1 M phosphate buffer containing glutaraldehyde at 2.5 % for 2 h. The scaffolds were then rinsed with PBS and distilled water and incubated in a 1% osmium tetroxide aqueous solution for 1 h at room temperature. Dehydration in increasing concentration of ethanol solutions was performed, followed by desiccation in hexamethyldisilazane. A coating of platinum was performed before analysis in a Zeiss EVO LS10 microscope.

Published in : International Journal of Pharmaceutics (2021), vol. 610, 121205
DOI: https://doi.org/10.1016/j.ijpharm.2021.121205
Status : Postprint (Author's version)

2.10. IN VIVO BIOCOMPATIBILITY STUDY

In vivo studies were also conducted by implanting the scaffolds into the brain of healthy rats to assess the potential toxicity of the scaffolds as well as their tendency to degrade in the brain environment. After implantation, brains were imaged by Magnetic Resonance Imaging (MRI) in order to obtain the volume of scaffolds at the beginning and end of the follow-up period.

2.10.1. IN VIVO IMPLANTATION OF NANOFIBROUS SCAFFOLDS INTO RAT BRAIN CORTEX

Fischer female rats aged 8-10 weeks were obtained from Janvier Labs (Le Genest-Saint-Isle, France). The protocol was approved by the Ethical Committee for Animal Experimentation of Pays de la Loire, France. Animals were anesthetized by intraperitoneal injection of a mixture of ketamine (100 mg/kg) and xylazine (13 mg/kg) and positioned in a Kopf stereotaxic instrument. A 10 mm-long incision was made along the midline to create access to the surface of the skull. Following this, a burr hole was drilled into the skull using a high-speed drill to expose the brain tissues underneath. A portion of the brain cortex was then cut using a biopsy punch device and subsequently removed using vacuum suction to create a cavity that was approximately 3 mm wide and 2 mm deep.

To facilitate the scaffold implantation process, the nanofibrous scaffolds (containing 10 mg blank NPs) were rolled and cut into cylinders of 2 mm wide and 2 mm tall. Following the implantation of the scaffold into the cavity, the wound was sutured, and the rats were allowed to awake without any further intervention. All rats became fully conscious and active between 1 and 2 h after surgery and did not display any sign of distress. In control rats, the same surgical procedure was also performed, but no scaffold was implanted. The study consisted of 6 rats, 3 implanted with scaffolds and 3 controls, and was intended for a shortterm follow-up of 7 days.

2.10.2. IN VIVO MRI

MRI analysis was performed on days 1 and 7 with a Bruker Biospec 70/20 system operating at 7 T, under isoflurane (0.5% 1 L/min O2) anesthesia, with the monitoring of respiratory parameters. T2-weighted images were acquired with a multispin echo sequence [FOV = 35 × 35 mm, 7 axial 0.8 mm slices (gap = 0.3 mm), matrix 256 × 256, TR = 2 s, 25 TE = 8, 16, 24... 200 ms, one average]. The volume of the scaffolds was measured by manually drawing the region of interest on the generated T2 maps.

2.10.3. STATISTICAL ANALYSIS

All data were expressed as the mean ± standard deviation of at least three experiments ($n \geq 3$). When applicable, one-way ANOVA with Dunnet's post-hoc test with a significance level of P equal to 0.05 was employed to detect any statistically significant difference existing between multiple data groups. In the figures, * indicates $P \leq 0.05$, ** indicates $P \leq 0.01$, *** indicates $P \leq 0.001$ and **** indicates $P \leq 0.0001$.

Published in : International Journal of Pharmaceutics (2021), vol. 610, 121205
DOI: https://doi.org/10.1016/j.ijpharm.2021.121205
Status : Postprint (Author's version)

3. Results

3.1. CHARACTERIZATION OF PROTEIN-LOADED NANOPARTICLES

Nanoparticles (NPs) were produced from PLGA and PEG-PLGA using a phase separation process to encapsulate the protein of interest. The synthesized NPs were mostly spherical (Figure 1) and uniform in size, as indicated by the low PDI values of the NP formulations (Table 1), regardless of the type of protein encapsulated. The slightly negative zeta-potential values can be explained by the presence of the hydrophilic PEG layer on the surface of the NPs that shields the negatively charged carboxyl groups carried by the hydrophobic PLGA forming the NP core (Haji Mansor et al., 2018). The NPs were also highly efficient in encapsulating lysozyme and SDF-1α (Table 1).

***Figure 1**. Scanning electron microscopy of (A) lysozyme-loaded and (B) SDF-1α-loaded nanoparticles.*

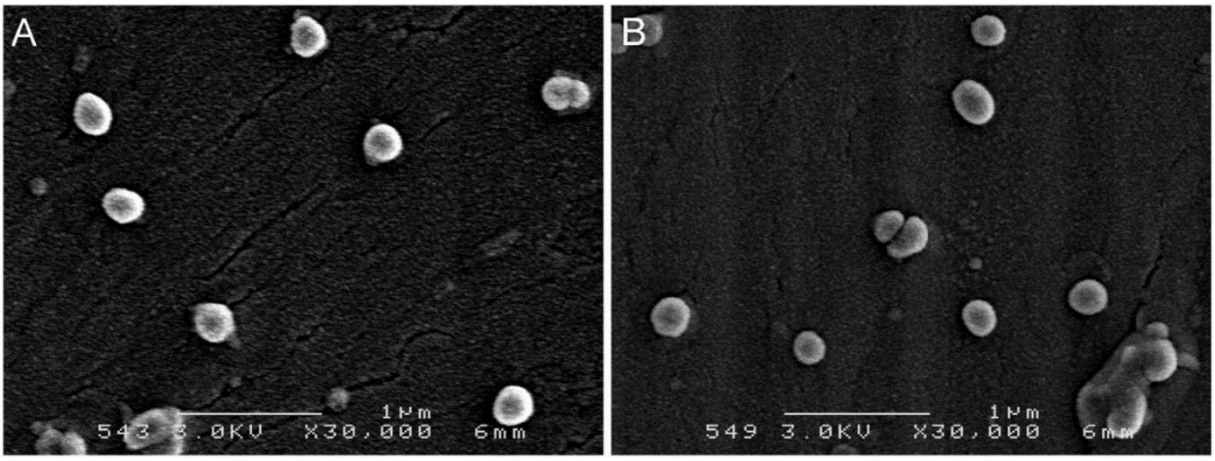

***Table 1**. Average size, polydispersity index (PDI), zeta-potential (ZP) and encapsulation efficiencies of lysozyme-loaded and SDF-1α-loaded nanoparticle formulations.*

Encapsulated protein	Average size (nm)[a]	Average PDI[a]	Average ZP (mV)[b]	Encapsulation efficiency (%)
Lysozyme	244±11	0.14±0.01	−4.1±0.7	96±5
SDF-1α	238±8	0.12±0.01	−3.5±0.6	87±5

[a] Purified nanoparticle dispersion was diluted to 100 µg/mL in deionized water prior to measurement.

[b] Purified nanoparticle dispersion was diluted to 100 µg/mL in 0.01 M NaCl solution, and the pH was adjusted to pH 7 prior to measurement.

Published in : International Journal of Pharmaceutics (2021), vol. 610, 121205
DOI: https://doi.org/10.1016/j.ijpharm.2021.121205
Status : Postprint (Author's version)

3.2. CHARACTERIZATION OF NANOPARTICLE-CONTAINING NANOFIBROUS SCAFFOLDS

3.2.1. CO-ELECTROSPINNING OF CHITOSAN AND PROTEIN-LOADED NANOPARTICLES

The electrospinning process produced flat scaffolds of approximately 40 µm thick after 165 min (Figure 2A). The presence of NPs in the scaffolds was initially confirmed using ATR-FTIR spectroscopy. ATR-FTIR spectra of scaffolds loaded with different concentrations of NPs revealed the presence of a peak at 1758 cm^{-1} (Figure 2B), which is characteristic of the ester bonds present in the PLGA component of the NP. In addition, as the NP load in the scaffolds was increased, the height of this peak increased proportionately (Figure 2B).

To gain an insight into the effect of different NP loads on the morphology of the electrospun nanofibers, SEM and TEM images of the scaffolds were recorded. SEM images revealed the presence of the NPs within the nanofibers as "bulges" that were visible along their lengths (Figure 2C), and these features became increasingly apparent as the NP load was increased from 4.0% w/w (5 mg of NPs) to 14.2% w/w (20 mg of NPs). Further observation using TEM confirmed the presence of spherical NPs within these "bulges" (Figure 2D). Interestingly, at the highest NP load tested (14.2% w/w), the nanofibers were found to be thinner (Table 2) and cut at random points (Figure 2 C&D, 20 mg NPs). Therefore, the maximum load of protein-loaded NPs in the nanofibrous scaffolds for further experiments was limited to 7.6% w/w (10 mg NPs per 121 mg chitosan-PEO mixture) to preserve good co-electrospinnability.

***Figure 2**. Characterization of nanofibrous scaffolds. (A) An example of nanofibrous scaffolds produced from the electrospinning process. The scale placed on the left displayed length in centimeters. (B) ATR-FTIR spectra of nanofibrous scaffolds with different nanoparticle loads. For each spectrum, the absorbance values were normalized to their corresponding highest absorbance value, which was recorded at 1557 cm^{-1}, to permit height comparison of the peak at 1758 cm^{-1}. (C) SEM and (D) TEM micrographs of nanofibrous scaffolds with different nanoparticle loads.*

Published in : International Journal of Pharmaceutics (2021), vol. 610, 121205
DOI: https://doi.org/10.1016/j.ijpharm.2021.121205
Status : Postprint (Author's version)

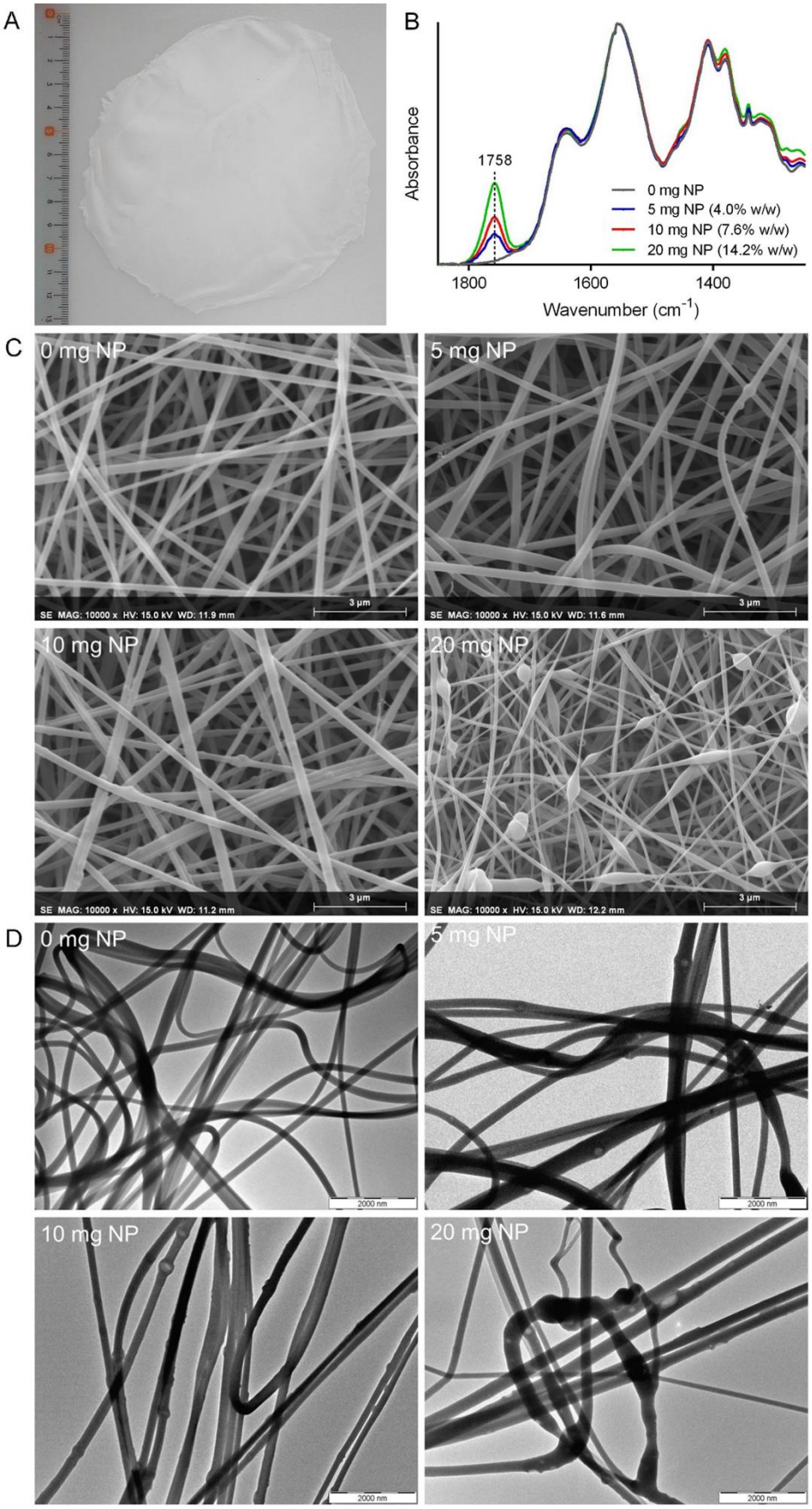

Published in : International Journal of Pharmaceutics (2021), vol. 610, 121205
DOI: https://doi.org/10.1016/j.ijpharm.2021.121205
Status : Postprint (Author's version)

***Table 2**. Fiber diameter of nanofibrous scaffolds with different nanoparticle loads.*

Nanoparticle load	Fiber diameter before stabilization (nm)[a]	Fiber diameter after stabilization (nm)[a]
0mg	249±49	263±42
5mg (4.0% w/w)	244±52	–
10mg (7.6% w/w)	251±46	261±45
20mg (14.0% w/w)	150±43	–

[a] Only the parts of the nanofibers that were free of the "bulges" were measured.

3.2.2. STABILIZATION OF NANOPARTICLE-CONTAINING NANOFIBROUS SCAFFOLDS

To reduce the solubility of the developed electrospun scaffolds, a stabilization step was implemented. The changes in the composition of the NP-containing nanofibrous scaffolds after the stabilization step were investigated using ATR-FTIR spectroscopy (Figure 3A). The procedure successfully deprotonated the chitosan amino groups as evidenced by the appearance of a peak at 1592 cm^{-1}, which correlated to the N-H stretching of the NH2 groups. The neutralization of the chitosan amino groups was accompanied by the disappearance of the peaks at 1557 and 1406 cm^{-1} originating from the asymmetric and symmetric stretching of the carboxylate component of acetate ions. In addition, the neutralization procedure increased the visibility of several chitosan characteristic peaks that were partially masked by the presence of the acetate ions. These include the trio of peaks at 1420, 1377 and 1322 cm-1 that represented CH_2 bending, CH_3 deformation and CH bending/CH_2 wagging respectively (Dong et al., 2001; Noriega and Subramanian, 2011). However, the peak at 1758 cm^{-1} that is characteristic of an ester bond as mentioned earlier remained visible after the stabilization procedure, suggesting that the PLGA/PEG-PLGA NPs were not significantly degraded by the 0.1 M NaOH neutralizing solution.

Using SEM, some degree of swelling can be observed in the stabilized nanofibers; however, the scaffold retained its overall nanofibrous morphology (Figure 3B).

Published in : International Journal of Pharmaceutics (2021), vol. 610, 121205
DOI: https://doi.org/10.1016/j.ijpharm.2021.121205
Status : Postprint (Author's version)

***Figure 3**. Scaffold stabilization. (A) ATR-FTIR spectra of a nanofibrous scaffold containing 10 mg NP load (7.6% w/w) before and after stabilization. (B) SEM micrograph of the stabilized NP-containing nanofibrous scaffold.*

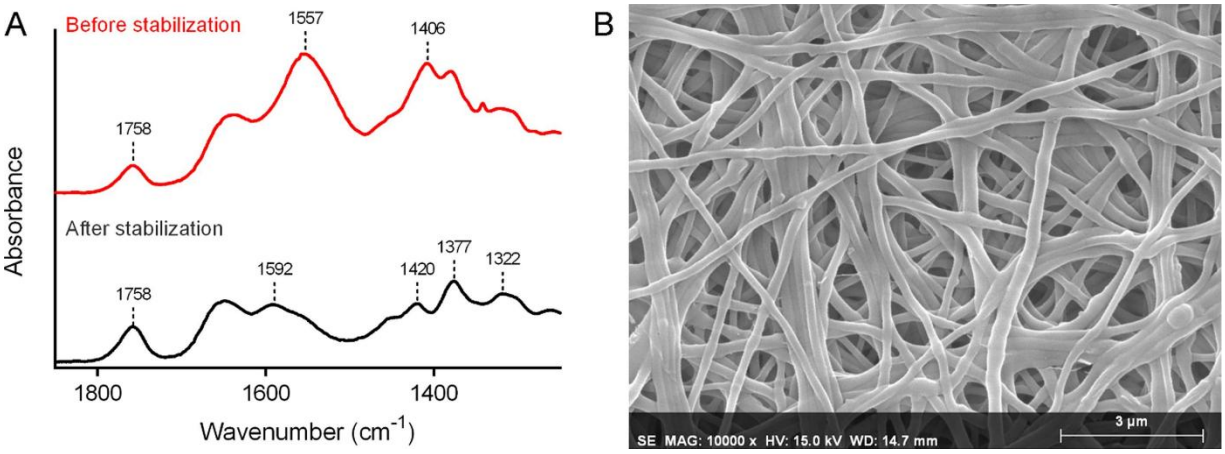

3.3. IN VITRO PROTEIN RELEASE STUDY

3.3.1. IN VITRO LYSOZYME RELEASE

The release of lysozyme from (i) the lysozyme-loaded NPs, (ii) the nanofibrous scaffold loaded with unencapsulated lysozyme molecules and (iii) the lysozyme-loaded NPs incorporated into a nanofibrous scaffold is shown in Figure 4A. Consistent with our previous finding (Haji Mansor et al., 2018), a steep initial release curve that plateaued after 3 days was obtained in the first case (Figure 4A, black line). A similar release profile was also observed in the second case, indicating that a direct dispersion of lysozyme molecules within the nanofibrous scaffold did not prevent the huge initial burst release (Figure 4A, blue line). After only 6 h, 39% of the bioactive unencapsulated lysozyme load was released. Then, the release tailed off drastically between 6 and 120 h and became negligible thereafter. Interestingly, in the third case, a more sustained release profile was observed (Figure 4A, red line). The scaffold prepared with lysozyme-loaded NPs released only 11% of its bioactive encapsulated lysozyme load after 6 h. This was followed by a gradual release that persisted up to day 35, the last time point of evaluation.

Figure 4**. In vitro protein release study and evaluation of SDF-1α bioactivity. (A) Cumulative release of lysozyme with respect to the amount of bioactive lysozyme retrievable from each sample (as quantified using the turbidity reduction assay). (B) Cumulative release of SDF-1α with respect to the amount of SDF-1α retrievable from each sample (as quantified using ELISA). (C) The distance of migration of CXCR4-expressing U87-MG cells induced by the SDF-1α-free medium (Blank), and medium supplemented with 40 ng/mL SDF-1α (native SDF-1α or those extracted just after electrospinning or released from nanofibrous scaffolds carrying either unencapsulated SDF-1α molecules (SDF-1α-NF) or SDF-1α-loaded nanoparticles (SDF-1α-NP-NF)). Statistical analysis was conducted to detect any significant difference ($P \leq 0.05$) between the multiple data groups; * indicates $P \leq 0.0001$. (D)*

Published in : International Journal of Pharmaceutics (2021), vol. 610, 121205
DOI: https://doi.org/10.1016/j.ijpharm.2021.121205
Status : Postprint (Author's version)

Representative images of CXCR4-expressing U87-MG cell-loaded agarose drops after 72-h incubation with SDF-1α-free medium (top left) or medium containing 40 ng/mL native SDF-1α (top right) or SDF-1α extracted after electrospinning (bottom left)/released (bottom right) from the nanofibrous scaffold containing SDF-1α-loaded NPs (day 20).

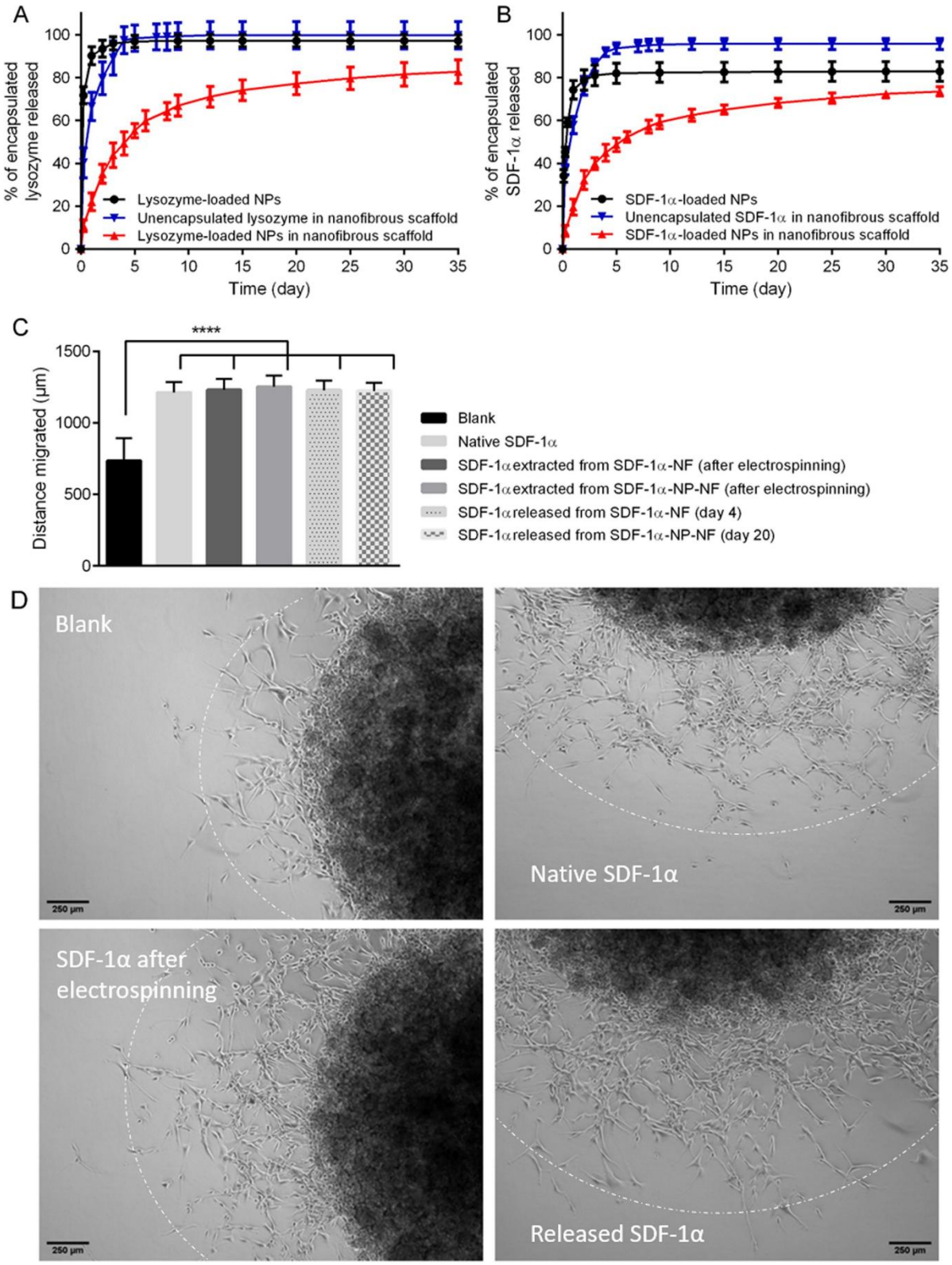

Published in : International Journal of Pharmaceutics (2021), vol. 610, 121205
DOI: https://doi.org/10.1016/j.ijpharm.2021.121205
Status : Postprint (Author's version)

3.3.2. IN VITRO SDF-1α RELEASE

SDF-1α release profiles were very similar to those observed with the model molecule lysozyme. The SDF-1α-loaded NPs and the nanofibrous scaffold loaded with unencapsulated SDF-1α (Figure 4B, black and blue lines, respectively) released most of their load steeply during the first three days of incubation and then leveled off with a negligible release after 5 days. In contrast, the nanofibrous scaffolds containing SDF-1α-loaded NPs provided a sustained release up to the last time point of evaluation, day 35 (Figure 4B, red line).

Having proved that a sustained release of the protein of interest was achieved, we then evaluated the biological activity of the released SDF-1α molecules using the agarose drop assay that we present next.

3.4. EVALUATION OF THE BIOLOGICAL ACTIVITY OF ELECTROSPUN AND RELEASED PROTEIN MOLECULES

In order to differentiate the effect of the scaffold fabrication process that involves high voltage conditions and the possible protein denaturation during the incubation times in the protein release studies, the biological activity of the model protein lysozyme and of SDF-1α both extracted just after the electrospinning step was assessed concomitant with the SDF-1α molecules obtained from the release studies from nanofibrous scaffolds carrying either i) unencapsulated SDF-1α molecules or ii) SDF-1α-loaded NPs.

3.4.1. EFFECT OF ELECTROSPINNING ON THE BIOLOGICAL ACTIVITY OF PROTEIN MOLECULES

Using the turbidity reduction assay, 93 ± 6% of the lysozyme molecules extracted from the nanofibrous scaffolds containing lysozyme-loaded NPs remained biologically active. This fraction decreased to 58 ± 4% when the lysozyme molecules were directly mixed with chitosan prior to electrospinning, highlighting the importance of lysozyme encapsulation into the NPs on the preservation of its bioactivity. It was also confirmed that the denaturation of the unencapsulated lysozyme molecules occurred mainly during the electrospinning process and not during their extraction from the nanofibrous scaffold, as there was negligible loss in their biological activity after successive incubations in 1 M acetic acid solution, which was used to dissolve the chitosan/PEO nanofibers, and 1 M NaOH solution, which was the solvent for the PLGA/PEG-PLGA NPs.

To investigate whether SDF-1α was also susceptible to electrospinning-induced denaturation, nanofibrous scaffolds containing either unencapsulated SDF-1α molecules or SDF-1α-loaded NPs were prepared. Using ELISA, there was no difference in the percentage recovery of SDF-1α from both types of scaffolds (94 ± 5% and 92 ± 4% from scaffolds loaded with unencapsulated SDF-1α molecules and those containing SDF-1α-loaded NPs, respectively). When the biological activity of the recovered SDF-1α molecules were assessed using the agarose drop migration assay, the distance of migration of CXCR4-expressing U87-MG cells induced by the SDF-1α molecules that were electrospun unencapsulated was similar to that induced by their encapsulated counterpart (Figure

Published in : International Journal of Pharmaceutics (2021), vol. 610, 121205
DOI: https://doi.org/10.1016/j.ijpharm.2021.121205
Status : Postprint (Author's version)

4C&D). In addition, no statistical difference was found as compared to the control drops incubated with native SDF-1α. These results suggest that SDF-1α was more resistant to electrospinning-induced denaturation than lysozyme.

3.4.2. EVALUATION OF THE BIOLOGICAL ACTIVITY OF THE RELEASED SDF-1α

The bioactivity of the SDF-1α molecules released from the nano-fibrous scaffolds was also assessed using the agarose drop migration assay. Release samples on day 4 from the nanofibrous scaffold loaded with unencapsulated SDF-1α molecules and on day 20 from the nanofibrous scaffold containing SDF-1α-loaded NPs were tested. These time points were chosen because the decrease in the release rate and the periodic refreshment of the release medium caused the amount of SDF-1α collected after these time points to be insufficient to achieve the optimal working concentration for the migration assay. SDF-1α molecules released from both scaffolds induced similar radial distances of CXCR4-expressing U87-MG cell migration compared to their pristine counterpart, and on average, a 1.8-fold increase in the radial cell migration distance relative to the negative control (Figure 4C&D). This increase in radial distance corresponds to approximately $(R_2/R_1)^2 = 1.8^2 = 3.24$-fold increase in the area of cell migration compared to control drops, assuming circular areas. These results suggest that the biological activity of SDF-1α molecules was retained during the release process regardless of whether they were encapsulated into NPs or not.

3.5. SCAFFOLD DEGRADATION STUDY

The degradation of the nanofibrous scaffolds was assessed by monitoring the loss of scaffold mass throughout incubation in a buffer solution supplemented with chitosan-degrading lysozyme. The degradation profiles were similar regardless of whether the scaffolds were loaded with blank NPs or not (Figure 5A, red and blue lines, respectively). Despite losing over 10% of their original mass after 5 weeks of incubation (Figure 5A), the scaffolds retained their nanofibrous structure as observed under SEM (Figure 5B).

Figure 5. *Degradability of scaffolds. (A) Percentage of original scaffold mass degraded with time of incubation in 0.05 M Tris-HCl buffer solution (pH 7.4) supplemented with 20 μg/mL lysozyme for the unloaded nanofibrous scaffolds (NF) and those loaded with 10 mg blank nanoparticles (Blank NP + NF). (B) SEM images of the unloaded nanofibrous scaffold (left) and the one loaded with 10 mg blank NP (right) after 5 weeks of incubation.*

Published in : International Journal of Pharmaceutics (2021), vol. 610, 121205
DOI: https://doi.org/10.1016/j.ijpharm.2021.121205
Status : Postprint (Author's version)

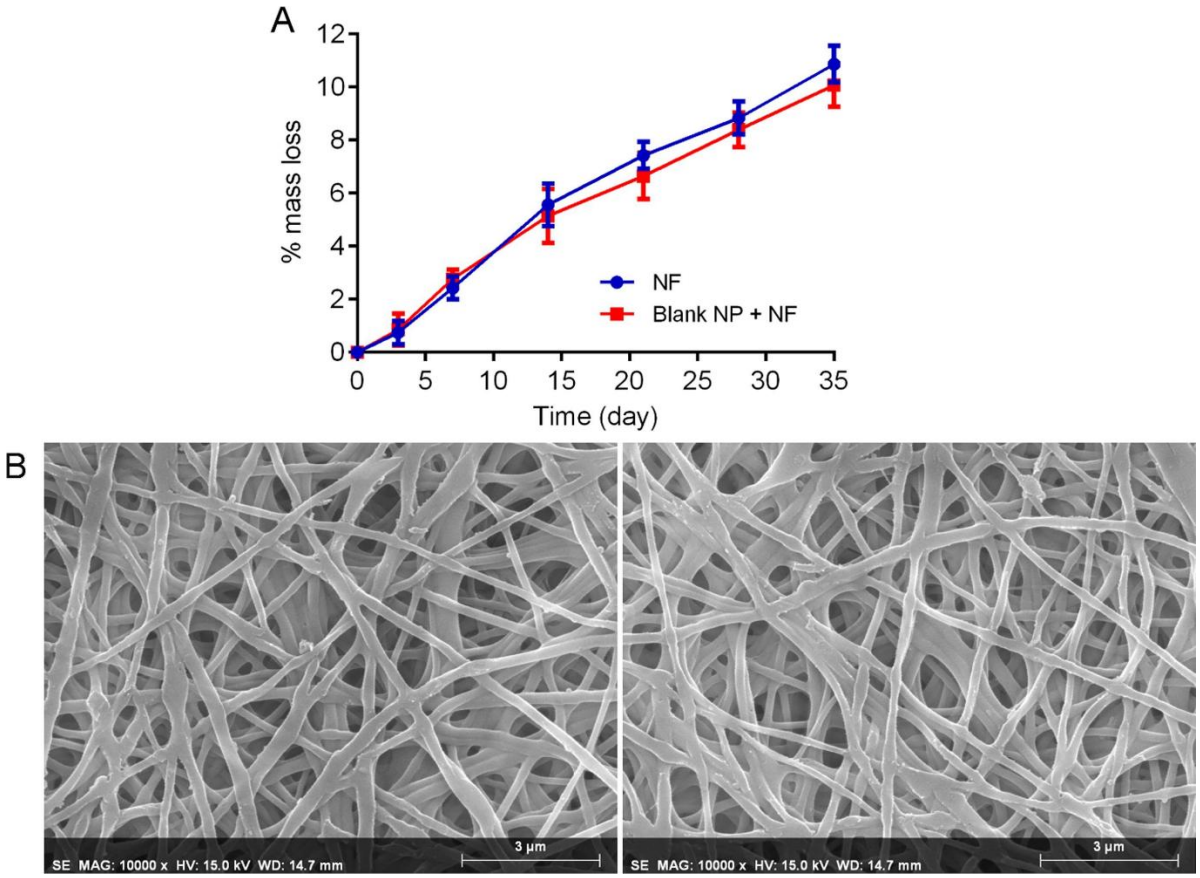

3.6. IN VITRO CYTOCOMPATIBILITY AND CELL ADHESION STUDY

In order to evaluate the cytocompatibility of the nanofibrous scaffolds NIH3T3 mouse fibroblast cells were incubated with conditioned medium that contained leached products from nanofibrous scaffolds loaded with blank NPs or not, released after a 24-h incubation period. Results show that after a 24-h treatment of NIH3T3 cells with this conditioned medium, no cytotoxicity was observed (Figure 6A), indicating that the leached compounds from both scaffold types were well-tolerated, in the short term, by the NIH3T3 cells.

To further extend the evaluation of the scaffold cytocompatibility, different cell lines comprising NIH3T3 mouse fibroblasts, Thp-1 macrophages, and primary astrocytes were directly incubated with scaffold circular punches of 10 and 14 mm in diameter; the latter corresponding to the double area of the former. Regardless of the surface area, both types of nanofibrous scaffolds, loaded with blank NPs or not, presented a light effect on the viability of cells in the short 24-h incubation time. This effect on viability was decreasing on average as follows: NIH3T3 mouse fibroblasts (83%) < Thp-1 macrophages (89%) < primary astrocytes (97%), for the nanofibers alone (NF, Figure 6B, 24 h); and, in the same cell order, 89% = 89% < 99%, for the nanofibers loaded with blank NPs (Blank NP + NF, Figure 6B, 24 h).

A similar trend was observed for the longer 72-h incubation period with results showing an average viability as follows: NIH3T3 mouse fibroblasts (74%) < Thp-1 macrophages (84%) < primary

Published in : International Journal of Pharmaceutics (2021), vol. 610, 121205
DOI: https://doi.org/10.1016/j.ijpharm.2021.121205
Status : Postprint (Author's version)

astrocytes (100%), for the nanofibers alone (NF, Figure 6B, 72 h); and, in the same cell order, 77% < 84% < 100%, for the nanofibers loaded with blank NPs (Blank NP + NF, Figure 6B, 72 h).

Finally, we evaluated the adhesion capacity of U87-MG cells on the nanofibrous scaffolds by depositing cells on top of scaffold sections for 4 h, followed by rinsing with PBS and incubation with routine culture medium for 24 h. Results showed that an average of 57 % of the cells adhered to both types of scaffolds, unloaded and NP loaded, relative to the control wells containing cells that adhered to the cell culture plastic surface (Figure 6C). Interestingly, the cells that attached to the scaffolds developed and extended their pseudopodia as observed in the SEM images in Figure 6D.

***Figure 6**. In vitro Cytocompatibility and cell adhesion capacity of scaffolds. (A) Indirect cytotoxicity: % viability of NIH3T3 cells treated for 24 h with conditioned medium containing leachables resulting from incubation with either unloaded nanofibrous scaffolds (NF) or those loaded with 10 mg blank nanoparticles (Blank NP + NF) normalized to the viability of cells treated with fresh medium (control). (B) Direct induced cytotoxicity: % viability of three different cell types including NIH3T3 mouse fibroblasts, Thp-1 macrophages and primary astrocytes that were cultivated in direct contact with scaffolds. Cells were incubated with either 79 or 154 mm^2 circular sections of unloaded nanofibrous scaffolds (NF) or those loaded with 10 mg blank nanoparticles (Blank NP + NF) for either 24 h or 72 h. % viability is relative to the control wells. (C) Absorbance at 450 nm proportional to the number of U87-MG cells attached to the control surface of the cell culture plate (CCP), NF and Blank NP + NF. Statistical analysis was conducted to detect any significant difference ($P \leq 0.05$) between the multiple data groups. * indicates $P \leq 0.05$. (D) SEM images showing the morphology of U87-MG cells attached to the surface of NF (left) and Blank NP + NF (right).*

Published in : International Journal of Pharmaceutics (2021), vol. 610, 121205
DOI: https://doi.org/10.1016/j.ijpharm.2021.121205
Status : Postprint (Author's version)

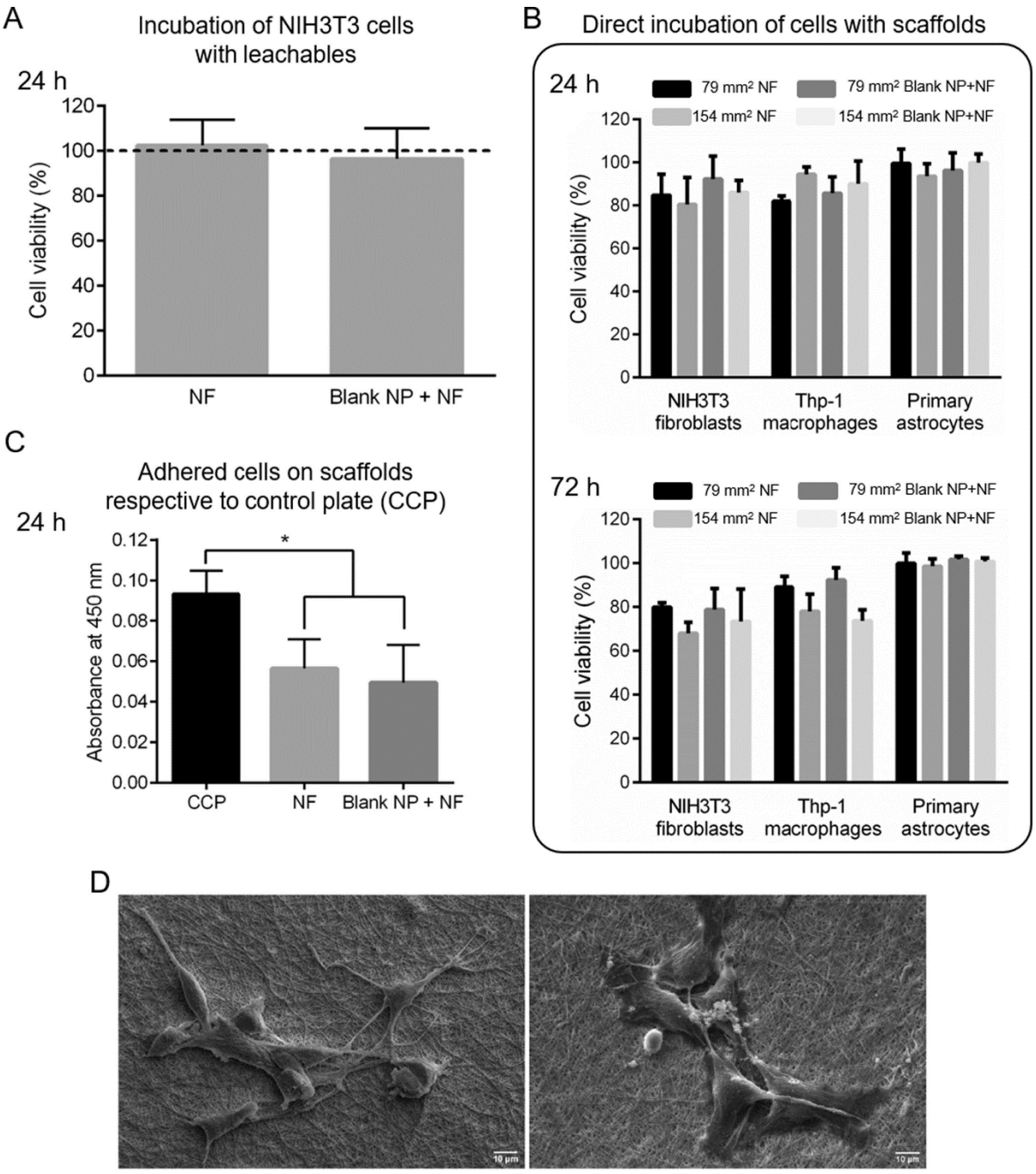

3.7. IN VIVO STUDY

In order to assess the biocompatibility of the blank-NP-loaded nanofibrous scaffolds *in vivo*, they were implanted as compacted rolls in the brain of healthy Fischer rats as described in section 2.10.1 and Figure 7. All animals, those carrying implants and controls bearing only the resection cavities, did not show any signs of distress, just after recovering from the surgery, and afterwards, during the course of the 7-day study. In addition, by assessing the implant volume by IRM at 1 day and 7 days after implantation no difference was observed in the calculated figures (Figure 7D). These results

Published in : International Journal of Pharmaceutics (2021), vol. 610, 121205
DOI: https://doi.org/10.1016/j.ijpharm.2021.121205
Status : Postprint (Author's version)

suggest an excellent biocompatibility and low degradation of scaffolds during the first week of treatment.

***Figure 7**. In vivo biocompatibility study. Nanofibrous scaffolds were rolled (A) and cut into compact cylinders of approximately 2 mm of height and 2 mm of diameter (B). Those rolled sections were then implanted in the resection cavity of healthy Fischer rats. The implanted scaffolds (C) were monitored by IRM 1 day and 7 days after implantation (only a representative MRI slice is shown). (D) Changes in the scaffold volume against the duration of implantation. The dotted line indicates the calculated dry volume of the scaffolds (6.3 mm^3). Paired t-test revealed no significant difference between the mean scaffold volume at day 1 and day 7 (p = 0.10).*

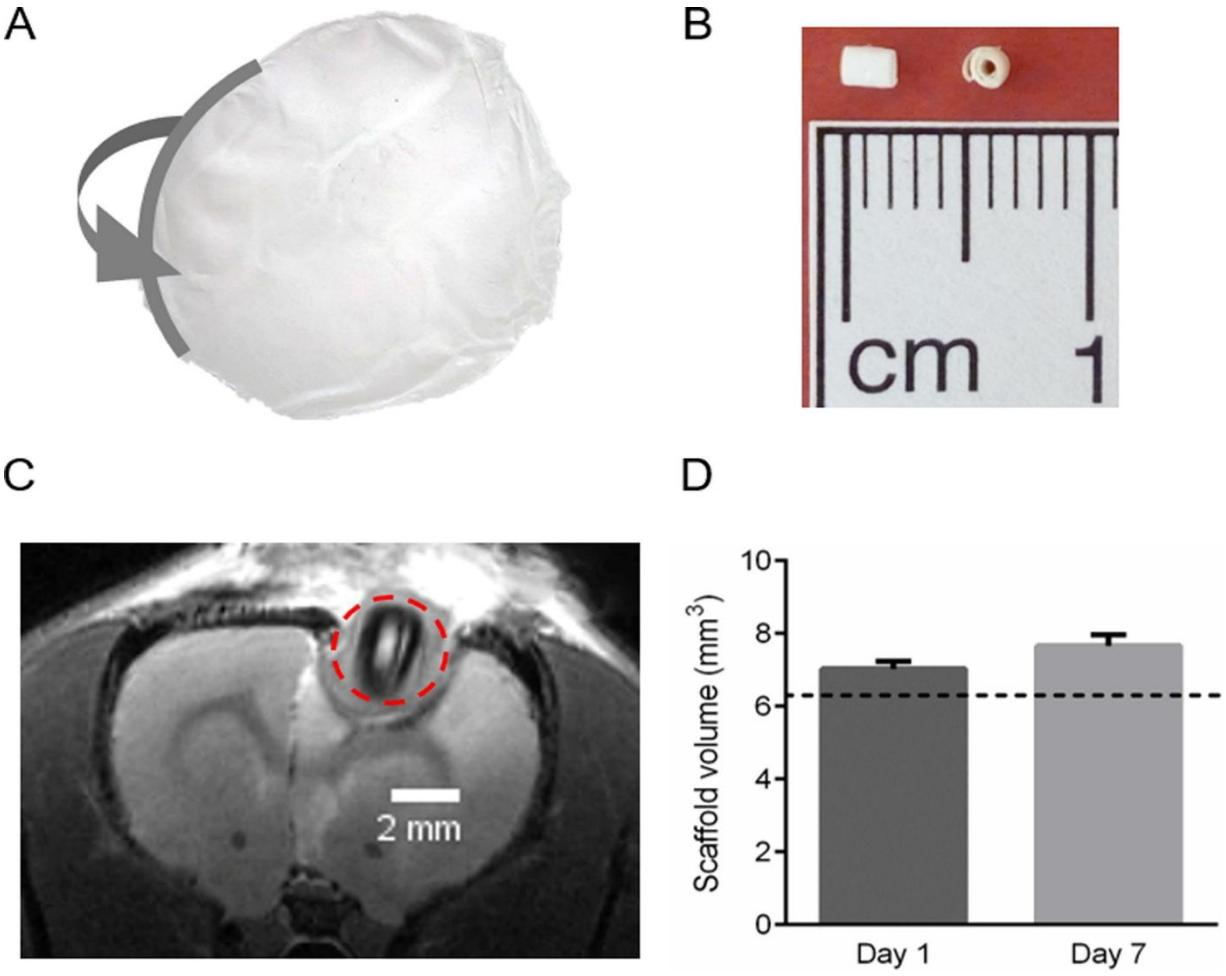

4. Discussion

Chemokines such as SDF-1α can mobilize cancer cells from their respective primary tumor locations towards proximal or distant colonizable sites by making them migrate up the chemokine concentration gradient (Carmo et al., 2010; Katsura et al., 2018; Kim et al., 2006; Roccaro et al., 2014;

Published in : International Journal of Pharmaceutics (2021), vol. 610, 121205
DOI: https://doi.org/10.1016/j.ijpharm.2021.121205
Status : Postprint (Author's version)

Zagzag et al., 2008). The implantation of SDF-1α-secreting scaffolds therefore opens the possibility of trapping these cells for subsequent selective killing procedures. This approach is highly relevant for treating cancers capable of metastasis, as the SDF-1α-secreting scaffolds may divert the cancer cells away from their conventional metastatic niches and disrupt the natural cancer progression.

More importantly, for cancers with high rates of local relapse due to an incomplete primary tumor removal such as glioblastoma, the trapping strategy could be used to eradicate the residual cancer cells and therefore prevent tumor recurrence. Recently, it was reported that a chemoattractant-loaded membrane could attract glioblastoma cells *in vitro*, despite the presence of several limitations that might have impaired the trapping capacity of the device, including short duration of chemoattractant release (Autier et al., 2018). In the present work, we developed scaffolds capable of providing sustained release of SDF-1α in its bioactive form with excellent cytocompatibility and capacity to interact with human glioblastoma cells, which are intended for future implantation into the tumor resection cavity in the brain.

To achieve sustained SDF-1α release, the chemokine was encapsulated into biodegradable PLGA/PEG-PLGA nanoparticles (NPs), which were subsequently incorporated into nanofibrous scaffolds by electrospinning. Regarding the first step, the straightforward phase separation technique employed in this study yielded particles of mostly uniform shape and size that favored their incorporation into the nanofibrous scaffolds. For the subsequent electrospinning process, chitosan was the material of choice for synthesizing the nanofibrous scaffolds due to its unique physicochemical properties. As it is a weakly-basic polysaccharide, chitosan is insoluble in aqueous solutions of physiological pH. However, in dilute acid solutions such as 1 M acetic acid, the amino groups of chitosan are protonated, making the chitosan macromolecules soluble and thus feasible for electrospinning (Croisier and Jerôme, 2013; Rinaudo et al., 1999). In addition, the positively charged amino groups may have facilitated the interaction between the chitosan molecules and the negatively-charged SDF-1α-loaded NPs to ensure a successful co-electrospinning process. Nevertheless, the use of chitosan alone would not have permitted the generation of defect-free nanofibers under mild conditions (Dilamian et al., 2013; Geng et al., 2005; Kriegel et al., 2009; Ziani et al., 2011). Studies have shown that the strong electrostatic repulsion between positively-charged chitosan molecules prevents sufficient chain entanglement that is necessary for nanofiber formation (Min et al., 2004). Therefore, a small amount of high molecular weight PEO was added to the chitosan solution to promote chain entanglement by virtue of the formation of hydrogen bonds between the ether oxygen of PEO and the amino hydrogen of chitosan (Pakravan et al., 2011).

Up to a NP load of 10 mg (7.6% w/w), uniform nanofibers can be obtained at room temperature in the presence of PEO at a concentration of approximately 8.8% of the total PEO/chitosan mass in the electrospinning mixture (Figure 2). The requirement for such a low concentration of the biologically-inert PEO ensures that the electrospun scaffolds were predominantly characterized by the useful biological properties of chitosan, including excellent cancer cell adhesion (Dhiman et al., 2004) and slow biodegradation (Cunha-Reis et al., 2007), which was subsequently proven in our *in vitro* and *in vivo* studies. However, when the NP load was increased to 20 mg, beaded nanofibers of smaller diameter were produced (Figure 2 & Table 2). It was likely that the large number of negatively-

Published in : International Journal of Pharmaceutics (2021), vol. 610, 121205
DOI: https://doi.org/10.1016/j.ijpharm.2021.121205
Status : Postprint (Author's version)

charged NPs interacting with the positively-charged chitosan molecules reduced the hydrogen bond interactions and chain entanglement between the chitosan and PEO molecules, leading to the formation of thin fibers with beaded morphology as reported in the literature (Kriegel et al., 2009). Despite this, we have shown that our electrospinning setup can ensure uniform incorporation of up to 10 mg of NPs into a nanofibrous scaffold made of 110 mg of chitosan and 11 mg of PEO. As long as this NP loading limit is not exceeded, the developed method can also produce uniform nanofibers capable of providing a robust anchoring platform that is suitable for the adhesion of glioblastoma cells.

After neutralizing the charged amino groups in the nanofibrous scaffolds to improve their stability in physiological media, we observed that scaffolds containing SDF-1α-loaded NPs can sustain the release of SDF-1α for a longer duration than SDF-1α-loaded NPs alone and scaffolds containing unencapsulated SDF-1α molecules (Figure 4B). This may be explained by a two-stepped process involved in the release of SDF-1α from the scaffolds containing SDF-1α-loaded NPs. SDF-1α molecules will have to first diffuse out of the NPs into the nanofibers before they could be released into the surrounding medium. The first stage of the diffusion process is likely to be rate-limiting as the positively-charged SDF-1α molecules will have to overcome their electrostatic interactions with the negatively-charged carboxyl groups of PLGA in the NPs (Balmert et al., 2015). These interactions can be disrupted by cations such as Na^+ (Pakulska et al., 2016) that were present at a physiologically-relevant concentration in the release medium on the condition that they first have to diffuse through the nanofiber to make contact with the NPs. Based on this assumption, it was not expected that SDF-1α release could be observed immediately after incubation in the release medium. A potential explanation for this observation is that some large NPs that were not completely embedded in the nanofibers, as visualized under SEM and TEM, were releasing part of their SDF-1α load immediately upon direct contact with the release medium. This stage of minimal burst release was then followed by the two-staged diffusion of SDF-1α from the NPs that were better embedded in the nanofibers as discussed above, contributing to gradual SDF-1α release.

As described earlier, the electrospinning step involves the use of high voltage to generate nanofibers. A strong electric field is needed to induce a repulsive force between the charged particles in a polymer solution to overcome the surface tension of the liquid that is necessary for the Taylor cone formation and subsequent fiber deposition on the collector plate (Ramakrishna et al., 2006). This harsh processing condition presents a significant barrier to the incorporation of protein molecules into electrospun scaffolds. Indeed, using lysozyme as a model protein, we observed that high voltage can denature more than 40% of the protein molecules that were electrospun directly without any prior encapsulation step. In contrast, the electrospinning process inflicted negligible loss of biological activity on lysozyme molecules that were pre-encapsulated into NPs. The protective effect of protein encapsulation may be explained by the immobilization of the protein molecules within the polymeric matrix of the NPs. In an electric field, dipole moments arising from individual domains within a protein molecule will be forced to align themselves along the applied field (Martin et al., 2018; Ojeda-May and Garcia, 2010; Ripoll et al., 2005). The movement of the polarized domains can alter the overall protein structure that may result in a loss of biological activity (Toschi et al., 2009; Wang et al., 2014; Zhao and Yang, 2009), particularly for enzymes such as

Published in : International Journal of Pharmaceutics (2021), vol. 610, 121205
DOI: https://doi.org/10.1016/j.ijpharm.2021.121205
Status : Postprint (Author's version)

lysozyme with a sensitive substrate binding site (Bekard and Dunstan, 2013; Zhao and Yang, 2010). Differently, encapsulated lysozyme molecules have limited conformational mobility due to their steric and electrostatic interactions with the polymeric constituents of the NP, preventing them from undergoing structural changes that can compromise their enzymatic activity. However, we also observed that SDF-1α retained its biological activity after the electrospinning process regardless of whether it was encapsulated or not. Although it was not possible to accurately quantify the proportion of bioactive SDF-1α due to the semi-quantitative nature of the agarose drop migration assay, it is probable that SDF-1α is more resistant to electrospinning-induced denaturation than lysozyme. This could be due to the difference in the secondary structure of these two proteins. Based on the information from Protein Data Bank (PDB 1DPX; PDB 2KEE), lysozyme possesses seven helices as opposed to two of SDF-1α. Helical domains are characterized by large net dipole moments due to their unidirectionally-aligned peptide dipoles (Hol, 1985; Wada, 1976), making them very reactive to an external electric field. In fact, lysozyme has been reported to unfold irreversibly upon exposure to an electric field of a strength as low as 300 V m^{-1} (Bekard and Dunstan, 2013). Considering the much stronger electric field applied in this study, it is plausible that lysozyme unfolded more extensively than SDF-1α when these proteins were electrospun non encapsulated.

Having proved that the protein of interest remained active just after the electrospinning process, we evaluated the bioactivity of SDF-1α after releasing into a medium resembling physiological characteristic, using an agarose drop assay. As stated before, the evaluated media corresponded to samples collected at day 4 and day 20 for the unencapsulated-SDF-1α-loaded scaffolds and the SDF-1α-loaded NP-containing scaffolds, respectively. After those points, SDF-1α was too diluted to obtain adequate working concentrations of the chemoattractant as the media was refreshed periodically at the defined time points. Interestingly, in spite of 20 days of incubation at 37 °C for the scaffolds containing SDF-1α-loaded NPs, the chemoattractant capacity of SDF-1α remained unaltered as observed over the effect on the cell-migrated radial distances and areas (1.8-fold and 3.24-fold increase, respectively) relative to controls without chemoattractant (Figure 4C&D). Based on these observations, the sustained release profile during the studied 5-week SDF-1α release period, together with the maintenance of the bioactivity of the released SDF-1α, are likely to provide a longer time window for glioblastoma cell trapping compared to the 2-day protein release duration achieved with the chemoattractant-loadable membranes developed by Autier and colleagues for a similar purpose (Autier et al., 2018).

To study the degradation of the nanofibrous scaffolds, lysozyme was the enzyme of choice as chitosan is hydrolyzed *in vivo* mainly via the action of this enzyme (Vårum et al., 1997). However, despite the exposure to lysozyme at a concentration comparable to the cerebrospinal fluid lysozyme levels of 1-14 µg⁄mL (Constantopoulos et al., 1976; Newman et al., 1974), the nanofibrous scaffolds remained mostly intact at the end of the degradation study (Figure 5). The slow degradation rate can be explained by the high degree of deacetylation (~80%) of the chitosan used to prepare the scaffolds. As lysozyme degrades chitosan by targeting its acetylated residues (Sashiwa et al., 1990), the degradation rate generally decreases with an increasing degree of chitosan deace-tylation (Freier et al., 2005; Ren et al., 2005). This slow degradation rate was also confirmed in the 7-day *in vivo* study, where the scaffolds volumes as assessed by MRI remained equal after 1 day and 7 days

Published in : International Journal of Pharmaceutics (2021), vol. 610, 121205
DOI: https://doi.org/10.1016/j.ijpharm.2021.121205
Status : Postprint (Author's version)

postimplantation. It is expected that the high stability of the scaffolds will be beneficial for holding the SDF-1α-loaded NPs in place during the gradual SDF-1α release process to permit the establishment of a local SDF-1α concentration gradient that is necessary for the chemotactic attraction of glioblastoma cells.

In addition, the scaffolds' nanofibrous feature was observed to be unaffected by their slow degradation rates (Figure 5B). It has been reported that surface structure significantly influences the extent of cell adhesion, and scaffolds with three-dimensional nanofibrous topography retain cancer cells to a greater degree than two-dimensional flat films (Du et al., 2011). As such, the robust nanofibrous structure suggests that our scaffolds can provide a cell-anchoring platform to retain the attracted glioblastoma cells until the subsequent killing step.

In our cell adhesion assay, U87-MG cells could spread well on the scaffold surface by extending their pseudopodia to maximize cellscaffold interactions (Figure 6C&D). However, there was minimal cell infiltration into the scaffolds due to the compact arrangement of the nanofibers. This dense structure resulted from the deposition of nanofibers over an aluminum sheet used as collector in the electrospinning process. This aspect may limit the GBM cell trapping capacity of the used electrospun scaffolds as cell migration requires matrix remodeling in pores of < 7 μm^2 in size (Wolf et al., 2013). Indeed, cancer cells including gliomas (Hagemann et al., 2012) or other cell types within the tumor microenvironment (Kessenbrock et al., 2010) often express high levels of matrix metalloproteinases to digest ECM components such as collagen, fibronectin and laminin to facilitate their invasion into surrounding healthy tissues. Considering that chitosan is not a native constituent of the ECM, it is unlikely that cancer cells such as those of GBM can enzymatically degrade chitosan-based scaffolds to infiltrate these constructs. In spite of this, our results suggest strong adhesion of cells as they remained attached on the scaffolds following 3 PBS washes after only 4 h passed from cell seeding. Should it become necessary to increase cell infiltration into the scaffolds to ameliorate their cell trapping capacity, the electrospinning technique can be improved to decrease the fiber density, by using for example custom-made collectors (Blakeney et al., 2011) and/or post-electrospinning treatments (Lee et al., 2005; Wu and Hong, 2016).

Finally, we evaluated the cytocompatibility of the scaffolds *in vitro* and *in vivo*. The implemented direct contact method provides a more realistic *in vitro* scenario. For that case, regardless of the surface area, both types of nanofibrous scaffolds (with and without blank NPs) were not highly toxic on any of the three cell lines tested (Figure 6B). This result was not surprising considering the well-reported biocompatibility of chitosan-based constructs (Mayerberger et al., 2018; Saravanan et al., 2018; Toullec et al., 2021; Tyliszczak et al., 2017; Wang et al., 2018). At the 24-h limit, the lowest percentage viability recorded was 80% and this value decreased to 68% at the 72-h limit. These figures were recorded when the larger-sized (154 mm2) NP-free scaffolds were put into contact with NIH3T3 fibroblasts, which are known to be highly sensitive to chemical-induced toxicities (Xia et al., 2008). It is worth mentioning that among the three cell lines tested, the brain-resident primary astrocytes appeared to be the most resistant against any toxic effects of the scaffolds, with an average percentage viability of 99%. This observation provides early evidence for the safe use of the nanofibrous scaffolds in the brain.

Published in : International Journal of Pharmaceutics (2021), vol. 610, 121205
DOI: https://doi.org/10.1016/j.ijpharm.2021.121205
Status : Postprint (Author's version)

Furthermore, slow-degrading chitosan scaffolds have also been reported to be more biocompatible than their fast-degrading counterparts due to the slower production of pro-inflammatory degradation products (Tomihata and Ikada, 1997). Therefore, the developed slow-degrading nanofiber scaffolds, coupled with the absence of cytotoxic leached compounds from the scaffolds observed in our cytocompatibility study (Figure 6A), may help to diminish the risk of an unfavorable immune or toxicological response during the several weeks of implantation period that will be necessary for maximizing the trapping of glioblastoma cells.

Lastly, we evaluated the biocompatibility of nanofibrous scaffolds *in vivo*. Flat electrospun chitosan scaffolds were rolled into cylinders before being implanted into the brain cortex. This approach increased the surface area for cell contact as cells may access the interior of the scaffolds by migrating from either the top or bottom of the construct. The absence of adverse effects on implanted rats during the 7-day evaluation period together with the slow biodegradability of scaffolds, encourage their use for their long-term evaluation. Overall, based on our results, the developed scaffolds may support prolonged duration of GBM cell trapping by acting as a stable reservoir for gradual SDF-1α release as well as by serving as a durable matrix to retain the recruited cells. The latter contribution is especially important as premature scaffold degradation may increase the risk of GBM cells being released back into the brain after their recruitment, which reduces the purpose of the scaffold to merely a "relay site", instead of a trap, for the GBM cells.

5. Conclusion

This study reports on the successful development of a novel chitosan-based nanofibrous scaffolds containing SDF-1α-loaded PLGA-based NPs to achieve sustained release of SDF-1α while keeping stable for at least 5 weeks *in vitro*. The scaffolds were also stable for at least 1 week *in vivo*. The usability of such a composite polymeric vehicle for local delivery of protein molecules of similar physicochemical characteristics to SDF-1α should be explored. More importantly, as the scaffolds demonstrated excellent *in vitro* and *in vivo* cytocompatibility and capacity to support the adhesion of glioblastoma cells *in vitro*, it is justifiable to proceed to the *in vivo* assessment of their bioperformace as a tumor cell trap for residual glioblastoma cells.

CRediT authorship contribution statement

Rodolfo Molina-Pena: Conceptualization, Methodology, Investigation, Writing - original draft. Muhammad Haji Mansor: Conceptualization, Methodology, Investigation, Writing - original draft. Mathie Najberg: Methodology, Investigation. Jean-Michel Thomassin: Methodology, Investigation, Writing - review & editing. Baya Gueza: Investigation. Carmen Alvarez-Lorenzo: Conceptualization, Method-ology, Writing - review & editing, Funding acquisition. Emmanuel Garcion: Conceptualization, Methodology, Writing - review & editing, Funding acquisition. Christine Jerôme: Conceptualization, Methodology, Writing - review & editing, Funding acquisition. Frank Boury: Conceptualization, Methodology, Writing - review & editing, Supervision, Project administration, Funding acquisition.

Published in : International Journal of Pharmaceutics (2021), vol. 610, 121205
DOI: https://doi.org/10.1016/j.ijpharm.2021.121205
Status : Postprint (Author's version)

Acknowledgements

Authors would like to thank R. Mallet and R. Perrot of the SCIAM (Common Service for Imaging and Microscopy Analysis, Angers, France) as well as V. Pitrebois and M. Dejeneffe of CERM for SEM and TEM analyses.

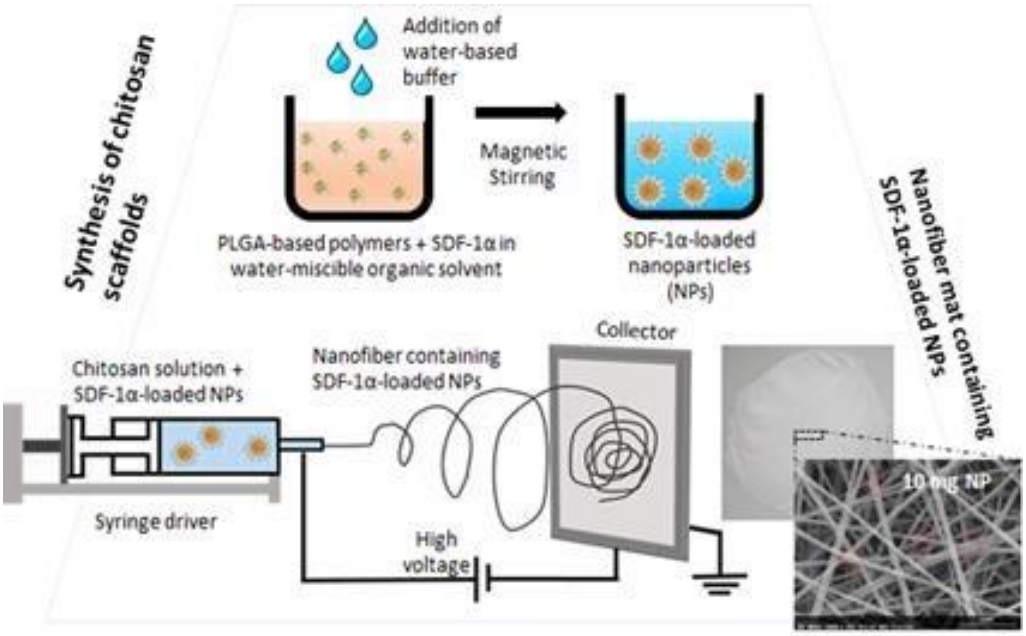

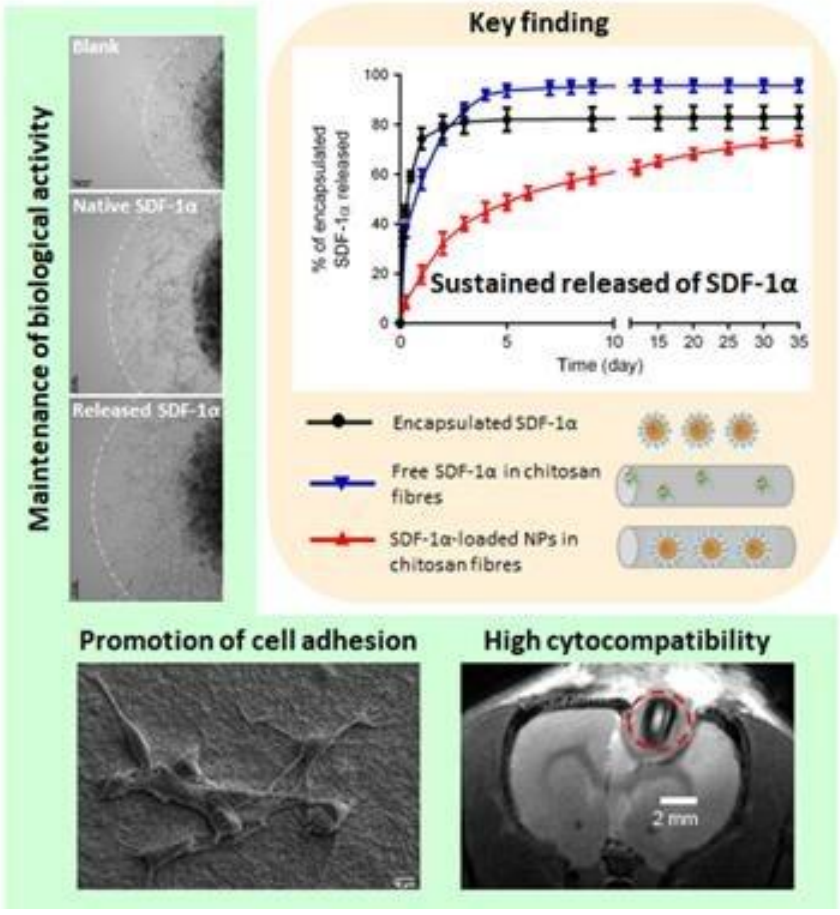

Published in : International Journal of Pharmaceutics (2021), vol. 610, 121205
DOI: https://doi.org/10.1016/j.ijpharm.2021.121205
Status : Postprint (Author's version)

References

Almouazen, E., Bourgeois, S., Boussaïd, A., Valot, P., Malleval, C., Fessi, H., Nataf, S., Briançon, S., 2012. Development of a nanoparticle-based system for the delivery of retinoic acid into macrophages. Int. J. Pharm. 430 (1-2), 207–215. https://doi.org/10.1016/j.ijpharm.2012.03.025.

Autier, L., Clavreul, A., Cacicedo, M.L., Franconi, F., Sindji, L., Rousseau, A., Perrot, R., Montero-Menei, C.N., Castro, G.R., Menei, P., 2018. A new glioblastoma cell trap for implantation after surgical resection. Acta Biomater. 84, 268–279. https://doi.org/10.1016/j.actbio.2018.11.027.

Balmert, S.C., Zmolek, A.C., Glowacki, A.J., Knab, T.D., Rothstein, S.N., Wokpetah, J.M., Fedorchak, M.V., Little, S.R., 2015. Positive charge of "sticky" peptides and proteins impedes release from negatively charged PLGA matrices. J. Mater. Chem. B 3 (23), 4723–4734. https://doi.org/10.1039/C5TB00515A.

Bekard, I., Dunstan, D.E., 2014. Electric field induced changes in protein conformation. Soft Matter 10 (3), 431–437. https://doi.org/10.1039/C3SM52653D.

Blakeney, B.A., Tambralli, A., Anderson, J.M., Andukuri, A., Lim, D.-J., Dean, D.R., Jun, H.-W., 2011. Cell infiltration and growth in a low density, uncompressed threedimensional electrospun nanofibrous scaffold. Biomaterials 32 (6), 1583–1590. https://doi.org/10.1016/j.biomaterials.2010.10.056.

Carmo, A.d., Patricio, I., Cruz, M.T., Carvalheiro, H., Oliveira, C.R., Lopes, M.C., 2010. CXCL12/CXCR4 promotes motility and proliferation of glioma cells. Cancer Biol. Ther. 9 (1), 56–65. https://doi.org/10.4161/cbt.9.1.10342.

Constantopoulos, A., Antonakakis, K., Matsaniotis, N., Kapsalakis, Z., 1976. Spinal Fluid Lysozyme in the Diagnosis of Central Nervous System Tumours. Neurochirurgia 19 (04), 169–171. https://doi.org/10.1055/s-0028-1090407.

Croisier, F., Jérôme, C., 2013. Chitosan-based biomaterials for tissue engineering. Eur. Polymer J., Biobased Polymers Related Mater. 49 (4), 780–792. https://doi.org/10.1016/j.eurpolymj.2012.12.009.

Cunha-Reis, C., TuzlaKoglu, K., Baas, E., Yang, Y., Haj, A.E., Reis, R.L., 2007. Influence of porosity and fibre diameter on the degradation of chitosan fibre-mesh scaffolds and cell adhesion. J. Mater. Sci. - Mater. Med. 18 (2), 195–200. https://doi.org/10.1007/s10856-006-0681-x.

De La Luz Sierra, M., Yang, F., Narazaki, M., Salvucci, O., Davis, D., Yarchoan, R., Zhang, H.H., Fales, H., Tosato, G., 2004. Differential processing of stromal-derived factor-1alpha and stromal-derived factor-1beta explains functional diversity. Blood 103, 2452–2459. https://doi.org/10.1182/blood-2003-08-2857.

Deng, J., Zou, Z.-M., Zhou, T.-l., Su, Y.-P., Ai, G.-P., Wang, J.-P., Xu, H., Dong, S.-w., 2011. Bone marrow mesenchymal stem cells can be mobilized into peripheral blood by G-CSF in vivo and integrate into traumatically injured cerebral tissue. Neurological Sci. 32 (4), 641–651. https://doi.org/10.1007/s10072-011-0608-2.

Dhiman, H.K., Ray, A.R., Panda, A.K., 2004. Characterization and evaluation of chitosan matrix for in vitro growth of MCF-7 breast cancer cell lines. Biomaterials 25 (21), 5147–5154. https://doi.org/10.1016/j.biomaterials.2003.12.025.

Dilamian, M., Montazer, M., Masoumi, J., 2013. Antimicrobial electrospun membranes of chitosan / poly (ethylene oxide) incorporating poly (hexamethylene biguanide) hydrochloride. Carbohydr. Polym. 94 (1), 364–371. https://doi.org/10.1016/j.carbpol.2013.01.059.

Dong, Y., Xu, C., Wang, J., Wang, M., Wu, Y., Ruan, Y., 2001. Determination of degree of substitution for N-acylated chitosan using IR spectra. Sci. China, Ser. B Chem. 44 (2), 216–224. https://doi.org/10.1007/BF02879541.

Du, J., Che, P.-L., Wang, Z.-Y., Aich, U., Yarema, K.J., 2011. Designing a binding interface for control of cancer cell adhesion via 3D topography and metabolic oligosaccharide engineering. Biomaterials 32 (23), 5427–5437. https://doi.org/10.1016/j.biomaterials.2011.04.005.

Du, L., Yang, S., Li, W., Li, H., Feng, S., Zeng, R., Yu, B., Xiao, L., Nie, H.Y., Tu, M., 2017. Scaffold composed of porous vancomycin-loaded poly(lactide-co-glycolide) microspheres: A controlled-release drug delivery system with shape-memory effect. Mater. Sci. Eng., C 78, 1172–1178. https://doi.org/10.1016/j.msec.2017.04.099.

Freier, T., Koh, H.S., Kazazian, K., Shoichet, M.S., 2005. Controlling cell adhesion and degradation of chitosan films by N-acetylation. Biomaterials 26 (29), 5872–5878. https://doi.org/10.1016/j.biomaterials.2005.02.033.

Frohbergh, M.E., Katsman, A., Botta, G.P., Lazarovici, P., Schauer, C.L., Wegst, U.G.K., Lelkes, P.I., 2012. Electrospun hydroxyapatite-containing chitosan nanofibers crosslinked with genipin for bone tissue engineering. Biomaterials 33 (36), 9167–9178. https://doi.org/10.1016/j.biomaterials.2012.09.009.

GENG, X., KWON, O., JANG, J., 2005. Electrospinning of chitosan dissolved in concentrated acetic acid solution. Biomaterials 26 (27), 5427–5432. https://doi.org/10.1016/j.biomaterials.2005.01.066.

Gentile, P., Nandagiri, V.K., Pabari, R., Daly, J., Tonda-Turo, C., Ciardelli, G., Ramtoola, Z., 2015. Influence of parathyroid hormone-loaded plga nanoparticles in porous scaffolds for bone regeneration. Int. J. Mol. Sci. 16, 20492–20510. https://doi.org/10.3390/ijms160920492.

Hagemann, C., Anacker, J., Ernestus, R.-I., Vince, G.H., 2012. A complete compilation of matrix metalloproteinase expression in human malignant gliomas. World J. Clin. Oncol. 3, 67–79. https://doi.org/10.5306/wjco.v3.i5.67.

Haji Mansor, M., Najberg, M., Contini, A., Alvarez-Lorenzo, C., Garcion, E., J´erˆome, C., Boury, F., 2018. Development of a Non-toxic and Non-denaturing Formulation Process for Encapsulation of SDF-1α into PLGA/PEG-PLGA Nanoparticles to Achieve Sustained Release. Eur. J. Pharm. Biopharm. 125, 38–50. https://doi.org/10.1016/j.ejpb.2017.12.020.

Hamoudeh, M., Salim, H., Barbos, D., Paunoiu, C., Fessi, H., 2007. Preparation and characterization of radioactive dirhenium decacarbonyl-loaded PLLA nanoparticles for radionuclide intra-tumoral therapy. Eur. J. Pharm. Biopharm. 67 (3), 597–611. https://doi.org/10.1016/j.ejpb.2007.04.003.

Hassani, L.N., Hindré, F., Beuvier, T., Calvignac, B., Lautram, N., Gibaud, A., Boury, F., 2013. Lysozyme encapsulation into nanostructured CaCO3 microparticles using a supercritical CO2 process and comparison with the normal route. J. Mater. Chem. B 1, 4011–4019. https://doi.org/10.1039/c3tb20467g.

He, Q., Ao, Q., Gong, Y., Zhang, X., 2011. Preparation of chitosan films using different neutralizing solutions to improve endothelial cell compatibility. J. Mater. Sci. Mater. Med. 22 (12), 2791–2802. https://doi.org/10.1007/s10856-011-4444-y.

Hol, W.G.J., 1985. The role of the α-helix dipole in protein function and structure. Prog. Biophys. Mol. Biol. 45 (3), 149–195. https://doi.org/10.1016/0079-6107(85)90001-X.

Huang, Z.-M., Zhang, Y.-Z., Kotaki, M., Ramakrishna, S., 2003. A review on polymer nanofibers by electrospinning and their applications in nanocomposites. Compos. Sci. Technol. 63 (15), 2223–2253. https://doi.org/10.1016/S0266-3538(03)00178-7.

Jin, F., Zhai, Q., Qiu, L., Meng, H., Zou, D., Wang, Y., Li, Q., Yu, Z., Han, J., Li, Q., Zhou, B., 2008. Degradation of BM SDF-1 by MMP-9: The role in G-CSF-induced hematopoietic stem/progenitor cell mobilization. Bone Marrow Transplant 42 (9), 581–588. https://doi.org/10.1038/bmt.2008.222.

Katsura, M., Shoji, F., Okamoto, T., Shimamatsu, S., Hirai, F., Toyokawa, G., Morodomi, Y., Tagawa, T., Oda, Y., Maehara, Y., 2018. Correlation between CXCR4/CXCR7/CXCL12 chemokine axis expression and prognosis in lymph-node-positive lung cancer patients. Cancer Sci. 109 (1), 154–165. https://doi.org/10.1111/cas.2018.109.issue-110.1111/cas.13422.

Kessenbrock, K., Plaks, V., Werb, Z., 2010. Matrix Metalloproteinases: Regulators of the Tumor Microenvironment. Cell 141 (1), 52–67. https://doi.org/10.1016/j.cell.2010.03.015.

Kim, J., Mori, T., Chen, S.L., Amersi, F.F., Martinez, S.R., Kuo, C., Turner, R.R., Ye, X., Bilchik, A.J., Morton, D.L., Hoon, D.S.B., 2006. Chemokine receptor CXCR4 expression in patients with melanoma and colorectal cancer liver metastases and the association with disease outcome. Ann. Surg. 244 (1), 113–120. https://doi.org/10.1097/01.sla.0000217690.65909.9c.

Kitaori, T., Ito, H., Schwarz, E.M., Tsutsumi, R., Yoshitomi, H., Oishi, S., Nakano, M., Fujii, N., Nagasawa, T., Nakamura, T., 2009. Stromal cell-derived factor 1/CXCR4 signaling is critical for the recruitment of mesenchymal stem cells to the fracture site during skeletal repair in a mouse model. Arthritis Rheum. 60 (3), 813–823. https://doi.org/10.1002/art.v60:310.1002/art.24330.

Knerlich-Lukoschus, F., Von Der Ropp-Brenner, B., Lucius, R., Mehdorn, H.M., Held-Feindt, J., 2010. Chemokine expression in the white matter spinal cord precursor niche after force-defined spinal cord contusion injuries in adult rats. Glia 58,916–931. https://doi.org/10.1002/glia.20974.

Kofuku, Y., Yoshiura, C., Ueda, T., Terasawa, H., Hirai, T., Tominaga, S., Hirose, M., Maeda, Y., Takahashi, H., Terashima, Y., Matsushima, K., Shimada, I., 2009. Structural basis of the interaction between chemokine stromal cell-derived factor-1/CXCL12 and its G-protein-coupled receptor CXCR4. J. Biol. Chem. 284 (50), 35240–35250. https://doi.org/10.1074/jbc.M109.024851.

Kriegel, C., Kit, K.M., McClements, D.J., Weiss, J., 2009. Electrospinning of chitosan poly (ethylene oxide) blend nanofibers in the presence of micellar surfactant solutions. Polymer 50 (1), 189–200. https://doi.org/10.1016/j.polymer.2008.09.041.

Lee, A.L.Z., Voo, Z.X., Chin, W., Ono, R.J., Yang, C., Gao, S., Hedrick, J.L., Yang, Y.Y., 2018. Injectable Coacervate Hydrogel for Delivery of Anticancer Drug-Loaded Nanoparticles in vivo. ACS Appl. Mater. Interfaces 10 (16), 13274–13282. https://doi.org/10.1021/acsami.7b14319.

Lee, Y.H., Lee, J.H., An, I.-G., Kim, C., Lee, D.S., Lee, Y.K., Nam, J.-D., 2005. Electrospun dual-porosity structure and biodegradation morphology of Montmorillonite reinforced PLLA nanocomposite scaffolds. Biomaterials 26 (16), 3165–3172. https://doi.org/10.1016/j.biomaterials.2004.08.018.

Ma, G., Liu, Y., Peng, C., Fang, D., He, B., Nie, J., 2011. Paclitaxel loaded electrospun porous nanofibers as mat potential application for chemotherapy against prostate cancer. Carbohydr. Polym. 86 (2), 505–512. https://doi.org/10.1016/j.carbpol.2011.04.082.

Marquez-Curtis, L., Jalili, A., Deiteren, K., Shirvaikar, N., Lambeir, A.-M., Janowska-Wieczorek, A., 2008. Carboxypeptidase M Expressed by Human Bone Marrow Cells Cleaves the C-Terminal Lysine of Stromal Cell-

Derived Factor-1α: Another Player in Hematopoietic Stem/Progenitor Cell Mobilization? Stem Cells 26 (5), 1211–1220. https://doi.org/10.1634/stemcells.2007-0725.

Martin, L.J., Akhavan, B., Bilek, M.M.M., 2018. Electric fields control the orientation of peptides irreversibly immobilized on radical-functionalized surfaces. Nat. Commun. 9, 357–367. https://doi.org/10.1038/s41467-017-02545-6.

Martínez Rivas, C.J., Tarhini, M., Badri, W., Miladi, K., Greige-Gerges, H., Nazari, Q.A., Galindo Rodríguez, S.A., Rom´an, R.´A., Fessi, H., Elaissari, A., 2017. Nanoprecipitation process: From encapsulation to drug delivery. Int. J. Pharm. 532 (1), 66–81. https://doi.org/10.1016/j.ijpharm.2017.08.064.

Mayerberger, E.A., Street, R.M., McDaniel, R.M., Barsoum, M.W., Schauer, C.L., 2018. Antibacterial properties of electrospun Ti3C2Tz (MXene)/chitosan nanofibers. RSC Adv. 8 (62), 35386–35394. https://doi.org/10.1039/C8RA06274A.

McCarthy, K.D., de Vellis, J., 1980. Preparation of separate astroglial and oligodendroglial cell cultures from rat cerebral tissue. J Cell Biol 85, 890–902. https://doi.org/10.1083/jcb.85.3.890.

Milner, R., Edwards, G., Streuli, C., Ffrench-Constant, C., 1996. A role in migration for the alpha V beta 1 integrin expressed on oligodendrocyte precursors. J. Neurosci.: The Off. J. Soc. Neurosci. 16, 7240–7252. https://doi.org/10.1523/JNEUROSCI.16-22-07240.1996.

Min, B.-M., Lee, S.W., Lim, J.N., You, Y., Lee, T.S., Kang, P.H., Park, W.H., 2004. Chitin and chitosan nanofibers: Electrospinning of chitin and deacetylation of chitin nanofibers. Polymer 45 (21), 7137–7142. https://doi.org/10.1016/j.polymer.2004.08.048.

Najberg, M., Haji Mansor, M., Taillé, T., Bouré, C., Molina-Peña, R., Boury, F., Cenis, J.L., Garcion, E., Alvarez-Lorenzo, C., 2020. Aerogel sponges of silk fibroin, hyaluronic acid and heparin for soft tissue engineering: Composition-properties relationship. Carbohydr. Polym. 237, 116107. https://doi.org/10.1016/j.carbpol.2020.116107.

Newman, J., Josephson, A.S., Cacatian, A., Tsang, A., 1974. Spinal-fluid lysozyme in the diagnosis of central-nervous-system tumors. Lancet 304, 756–757. https://doi.org/10.1016/S0140-6736(74)90946-5.

Nicolas, S., Bolzinger, M.-A., Jordheim, L.P., Chevalier, Y., Fessi, H., Almouazen, E., 2018. Polymeric nanocapsules as drug carriers for sustained anticancer activity of calcitriol in breast cancer cells. Int. J. Pharm. 550 (1-2), 170–179. https://doi.org/10.1016/j.ijpharm.2018.08.022.

Noriega, S.E., Subramanian, A., 2011. Consequences of Neutralization on the Proliferation and Cytoskeletal Organization of Chondrocytes on Chitosan-Based Matrices. Int. J. Carbohydrate Chem. 2011, 1–13. https://doi.org/10.1155/2011/809743.

O'Boyle, G., Swidenbank, I., Marshall, H., Barker, C.E., Armstrong, J., White, S.A., Fricker, S.P., Plummer, R., Wright, M., Lovat, P.E., 2013. Inhibition of CXCR4-CXCL12 chemotaxis in melanoma by AMD11070. Br. J. Cancer 108 (8), 1634–1640. https://doi.org/10.1038/bjc.2013.124.

Ojeda-May, P., Garcia, M.E., 2010. Electric field-driven disruption of a native β-sheet protein conformation and generation of a helix-structure. Biophys. J. 99 (2), 595–599. https://doi.org/10.1016/j.bpj.2010.04.040.

Ono, R.J., Lee, A.L.Z., Voo, Z.X., Venkataraman, S., Koh, B.W., Yang, Y.Y., Hedrick, J.L., 2017. Biodegradable Strain-Promoted Click Hydrogels for Encapsulation of Drug-Loaded Nanoparticles and

Sustained Release of Therapeutics. Biomacromolecules 18(8), 2277–2285. https://doi.org/10.1021/acs.biomac.7b00377.

Pakravan, M., Heuzey, M.-C., Ajji, A., 2011. A fundamental study of chitosan/PEO electrospinning. Polymer 52 (21), 4813–4824. https://doi.org/10.1016/j.polymer.2011.08.034.

Pakulska, M.M., Elliott Donaghue, I., Obermeyer, J.M., Tuladhar, A., McLaughlin, C.K., Shendruk, T.N., Shoichet, M.S., 2016. Encapsulation-free controlled release: Electrostatic adsorption eliminates the need for protein encapsulation in PLGA nanoparticles. Sci. Adv. 2, e1600519–e1600528. https://doi.org/10.1126/sciadv.1600519.

Pardridge, W.M., 2011. Drug transport in brain via the cerebrospinal fluid. Fluids Barriers CNS 8, 7–10. https://doi.org/10.1186/2045-8118-8-7.

Pham, Q.P., Sharma, U., Mikos, A.G., 2006. Electrospinning of polymeric nanofibers for tissue engineering applications: a review. Tissue Eng. 12 (5), 1197–1211. https://doi.org/10.1089/ten.2006.12.1197.

Pulavendran, S., Thiyagarajan, G., 2011. Three-dimensional scaffold containing EGF incorporated biodegradable polymeric nanoparticles for stem cell based tissue engineering applications. Biotechnol. Bioprocess Eng. 16 (2), 393–399. https://doi.org/10.1007/s12257-009-3155-4.

Ramakrishna, S., Fujihara, K., Teo, W.-E., Yong, T., Ma, Z., Ramaseshan, R., 2006. Electrospun nanofibers: Solving global issues. Mater. Today 9 (3), 40–50. https://doi.org/10.1016/S1369-7021(06)71389-X.

Ratajczak, M.Z., Kucia, M., Reca, R., Majka, M., Janowska-Wieczorek, A., Ratajczak, J., 2004. Stem cell plasticity revisited: CXCR4-positive cells expressing mRNA for early muscle, liver and neural cells "hide out" in the bone marrow. Leukemia 18 (1), 29–40. https://doi.org/10.1038/sj.leu.2403184.

Ren, D., Yi, H., Wang, W., Ma, X., 2005. The enzymatic degradation and swelling properties of chitosan matrices with different degrees of N-acetylation. Carbohydr. Res. 340 (15), 2403–2410. https://doi.org/10.1016/j.carres.2005.07.022.

Rinaudo, M., Pavlov, G., Desbrières, J., 1999. Influence of acetic acid concentration on the solubilization of chitosan. Polymer 40 (25), 7029–7032. https://doi.org/10.1016/S0032-3861(99)00056-7.

Ripoll, D.R., Vila, J.A., Scheraga, H.A., 2005. On the orientation of the backbone dipoles in native folds. Proc. Natl. Acad. Sci. 102 (21), 7559–7564. https://doi.org/10.1073/pnas.0502754102.

Roccaro, A., Sacco, A., Purschke, W., Moschetta, M., Buchner, K., Maasch, C., Zboralski, D., Z¨ollner, S., Vonhoff, S., Mishima, Y., Maiso, P., Reagan, M., Lonardi, S., Ungari, M., Facchetti, F., Eulberg, D., Kruschinski, A., Vater, A., Rossi, G., Klussmann, S., Ghobrial, I., 2014. SDF-1 inhibition targets the bone marrow niche for cancer therapy. Cell Reports 9 (1), 118–128. https://doi.org/10.1016/j.celrep.2014.08.042.

Saravanan, S., Sareen, N., Abu-El-Rub, E., Ashour, H., Sequiera, G.L., Ammar, H.I., Gopinath, V., Shamaa, A.A., Sayed, S.S.E., Moudgil, M., Vadivelu, J., Dhingra, S., 2018. Graphene Oxide-Gold Nanosheets Containing Chitosan Scaffold Improves Ventricular Contractility and Function After Implantation into Infarcted Heart. Sci. Rep. 8, 15069. https://doi.org/10.1038/s41598-018-33144-0.

Sashiwa, H., Saimoto, H., Shigemasa, Y., Ogawa, R., Tokura, S., 1990. Lysozyme susceptibility of partially deacetylated chitin. Int. J. Biol. Macromol. 12 (5), 295–296. https://doi.org/10.1016/0141-8130(90)90016-4.

Séhédic, D., Chourpa, I., Tétaud, C., Griveau, A., Loussouarn, C., Avril, S., Legendre, C., Lepareur, N., Wion, D., Hindré, F., Davodeau, F., Garcion, E., 2017. Locoregional Confinement and Major Clinical Benefit of ^{188}

Re-Loaded CXCR4-Targeted Nanocarriers in an Orthotopic Human to Mouse Model of Glioblastoma. Theranostics 7 (18), 4517–4536. https://doi.org/10.7150/thno.19403.

Sobolik, T., Su, Y.-J., Wells, S., Ayers, G.D., Cook, R.S., Richmond, A., Yap, A., 2014. CXCR4 drives the metastatic phenotype in breast cancer through induction of CXCR2 and activation of MEK and PI3K pathways. Mol. Biol. Cell 25 (5), 566–582. https://doi.org/10.1091/mbc.e13-07-0360.

Tchemtchoua, V.T., Atanasova, G., Aqil, A., Filée, P., Garbacki, N., Vanhooteghem, O., Deroanne, C., Noël, A., Jérôme, C., Nusgens, B., Poumay, Y., Colige, A., 2011. Development of a Chitosan Nanofibrillar Scaffold for Skin Repair and Regeneration. Biomacromolecules 12 (9), 3194–3204. https://doi.org/10.1021/bm200680q.

Tomihata, K., Ikada, Y., 1997. In vitro and in vivo degradation of films of chitin and its deacetylated derivatives. Biomaterials 18 (7), 567–575. https://doi.org/10.1016/S0142-9612(96)00167-6.

Toschi, F., Lugli, F., Biscarini, F., Zerbetto, F., 2009. Effects of Electric Field Stress on a β-Amyloid Peptide. J. Phys. Chem. B 113 (1), 369–376. https://doi.org/10.1021/jp807896g.

Toullec, C., Le Bideau, J., Geoffroy, V., Halgand, B., Buchtova, N., Molina-Peña, R., Garcion, E., Avril, S., Sindji, L., Dube, A., Boury, F., Jérôme, C., 2021. Curdlan-Chitosan Electrospun Fibers as Potential Scaffolds for Bone Regeneration. Polymers 13, 526. https://doi.org/10.3390/polym13040526.

Tyliszczak, B., Drabczyk, A., Kudłacik-Kramarczyk, S., Bialik-Wąs, K., Sobczak-Kupiec, A., 2017. In vitro cytotoxicity of hydrogels based on chitosan and modified with gold nanoparticles. J. Polym. Res. 24, 153. https://doi.org/10.1007/s10965-017-1315-3.

Vårum, K.M., Myhr, M.M., Hjerde, R.J.N., Smidsrød, O., 1997. In vitro degradation rates of partially N-acetylated chitosans in human serum. Carbohydr. Res. 299 (1-2), 99–101. https://doi.org/10.1016/S0008-6215(96)00332-1.

Wada, A., 1976. The alpha-helix as an electric macro-dipole. Adv. Biophys. 9, 1–63.

Wang, M.O., Etheridge, J.M., Thompson, J.A., Vorwald, C.E., Dean, D., Fisher, J.P., 2013. Evaluation of the In Vitro Cytotoxicity of Cross-Linked Biomaterial. Biomacromolecules 14, 1321–1329. https://doi.org/10.1021/bm301962f.

Wang, X., Guan, J., Zhuang, X., Li, Z., Huang, S., Yang, J., Liu, C., Li, F., Tian, F., Wu, J., Shu, Z., 2018. Exploration of Blood Coagulation of N-Alkyl Chitosan Nanofiber Membrane in Vitro. Biomacromolecules 19 (3), 731–739. https://doi.org/10.1021/acs.biomac.7b01492.

Wang, X., Li, Y., He, X., Chen, S., Zhang, J.Z.H., 2014. Effect of strong electric field on the conformational integrity of insulin. J. Phys. Chem. A 118 (39), 8942–8952. https://doi.org/10.1021/jp501051r.

Wolf, K., Te Lindert, M., Krause, M., Alexander, S., Te Riet, J., Willis, A.L., Hoffman, R. M., Figdor, C.G., Weiss, S.J., Friedl, P., 2013. Physical limits of cell migration: control by ECM space and nuclear deformation and tuning by proteolysis and traction force. J. Cell Biol. 201, 1069–1084. https://doi.org/10.1083/jcb.201210152.

Wu, J., Hong, Y.i., 2016. Enhancing cell infiltration of electrospun fibrous scaffolds in tissue regeneration. Bioact. Mater. 1 (1), 56–64. https://doi.org/10.1016/j.bioactmat.2016.07.001.

Xia, M., Huang, R., Witt, K.L., Southall, N., Fostel, J., Cho, M.-H., Jadhav, A., Smith, C.S., Inglese, J., Portier, C.J., Tice, R.R., Austin, C.P., 2008. Compound Cytotoxicity Profiling Using Quantitative High-Throughput Screening. Environ Health Perspect 116 (3), 284–291. https://doi.org/10.1289/ehp.10727.

Published in : International Journal of Pharmaceutics (2021), vol. 610, 121205
DOI: https://doi.org/10.1016/j.ijpharm.2021.121205
Status : Postprint (Author's version)

Xie, Z., Paras, C.B., Weng, H., Punnakitikashem, P., Su, L.-C., Vu, K., Tang, L., Yang, J., Nguyen, K.T., 2013. Dual growth factor releasing multi-functional nanofibers for wound healing. Acta Biomater. 9 (12), 9351–9359. https://doi.org/10.1016/j.actbio.2013.07.030.

Zagzag, D., Esencay, M., Mendez, O., Yee, H., Smirnova, I., Huang, Y., Chiriboga, L., Lukyanov, E., Liu, M., Newcomb, E.W., 2008. Hypoxia- and Vascular Endothelial Growth Factor-Induced Stromal Cell-Derived Factor-1α/CXCR4 Expression in Glioblastomas. Am. J. Pathol. 173 (2), 545–560. https://doi.org/10.2353/ajpath.2008.071197.

Zhang, H., Tian, Y., Zhu, Z., Xu, H., Li, X., Zheng, D., Sun, W., 2016. Efficient antitumor effect of co-drug-loaded nanoparticles with gelatin hydrogel by local implantation. Sci. Rep. 6, 1–14. https://doi.org/10.1038/srep26546.

Zhao, W., Yang, R., 2010. Experimental Study on Conformational Changes of Lysozyme in Solution Induced by Pulsed Electric Field and Thermal Stresses. J. Phys. Chem. B 114 (1), 503–510. https://doi.org/10.1021/jp9081189.

Zhao, W., Yang, R., 2009. Effect of high-intensity pulsed electric fields on the activity, conformation and self-aggregation of pepsin. Food Chem. 114 (3), 777–781. https://doi.org/10.1016/j.foodchem.2008.10.016.

Ziani, K., Henrist, C., Jérôme, C., Aqil, A., Maté, J.I., Cloots, R., 2011. Effect of nonionic surfactant and acidity on chitosan nanofibers with different molecular weights. Carbohydr. Polym. 83 (2), 470–476. https://doi.org/10.1016/j.carbpol.2010.08.002.